

## Modeling of decadal scale phosphorus retention in lake sediment under varying redox conditions

Sergei Katsev<sup>a,c</sup>, Maria Dittrich<sup>b,c,\*</sup>

<sup>a</sup> Large Lakes Observatory and Department of Physics, University of Minnesota Duluth, 2205 E. 5th Street, Duluth, MN 55812, USA

<sup>b</sup> Department of Physical and Environmental Sciences, University of Toronto Scarborough, 1265 Military Trail, Toronto, ON M1C 1A4, Canada

<sup>c</sup> Swiss Institute for Aquatic Science and Technology (Eawag), Kastanienbaum, Switzerland

### ARTICLE INFO

#### Article history:

Received 15 August 2012

Received in revised form 6 December 2012

Accepted 7 December 2012

Available online 29 January 2013

#### Keywords:

Early diagenesis

Nutrients

Reaction-transport modeling

Hypolimnion aeration

Restoration

Lake sediment

### ABSTRACT

Phosphorus (P) releases from lake sediments are controlled in the long term by P burial into the deep sediment and on shorter time scales by the redox conditions at the sediment–water interface. In Lake Sempach (Switzerland), hypolimnetic oxygen concentration was increased by artificial aeration after two decades of nearly anoxic conditions. Using diagenetic reaction-transport modeling and sediment core analysis, we investigated the effects that this change, as well as variations in the organic carbon loadings, had on the long-term mobility of sediment P. During low-oxygen conditions, the reducible iron pool in the sediment was depleted, resulting in the release of previously accumulated P. The remobilization of iron-bound P affected phosphate effluxes from the sediment on the time scale of the sediment iron cycle (several years). On longer time scales, P effluxes followed the sedimentation fluxes of organic matter. Mass balance calculations indicate that, despite the dominance of internal P loading in Lake Sempach, over the long-term phosphorus content in the water column was controlled by the external P inputs. The results suggest that, whereas short-term decreases in sediment P releases may be achieved by preventing sediment anoxia, long-term solutions should involve reductions in the external P inputs.

© 2012 Elsevier B.V. All rights reserved.

### 1. Introduction

Sediment composition and chemical fluxes respond to the variations in temperature, sedimentation fluxes, and the composition of bottom water on multiple time scales (Lasaga and Holland, 1976; Burdige, 2006). Perhaps the strongest changes arise from alterations to the sediment redox balance, i.e. the balance between the amounts of reductants and oxidants delivered to the sediment. In particular, variations in the bottom water oxygen levels and sedimentation fluxes of organic matter may substantially alter the pathways of mineralization and vertical distribution of sediment redox sensitive elements (Sundby et al., 1986; Katsev et al., 2006a). Depletion of oxygen may rid the sediment of iron and manganese oxides and lead to the accumulation of sulfides, as well as decreased benthic bioturbation (Dittrich et al., 2009). Because the diagenetic mobility of P, a productivity-controlling nutrient, is strongly affected by its association with iron oxyhydroxides (Boström et al., 1982; Sondergaard et al., 2001), maintaining an oxic sediment–water interface (SWI) was often suggested as a

means to curtail sediment P effluxes (Gächter and Imboden, 1985; Schauser et al., 2003). The long-term P retention, however, proved to be insensitive to the artificial oxygenation of bottom waters (Gächter and Wehrli, 1998). To explain this insensitivity, (Katsev et al., 2006b) argued that the relative importance of P mobilization mechanisms varies with the time scale of interest, the idea that was further corroborated in a recent review (Hupfer and Lewandowski, 2008). According to this argument, the classical paradigm of Einsele (1936) and Mortimer (1941), which treats seasonal P mobilization as redox-sensitive, should not be applied on greater time scales. The balance between the P sedimentation and its burial into the anoxic sediment has to be considered instead.

In this paper, we analyze the retention of P in the sediments of Lake Sempach (Switzerland) where bottom waters were artificially aerated after several decades of nearly anoxic conditions. We analyze temporal changes in sediment composition, organic matter mineralization pathways and diffusive fluxes across the sediment–water interface, and also identify processes that control P availability.

### 2. Site description and history

Lake Sempach is a pre-alpine hard water lake in central Switzerland (Table 1). It is stratified between April and October

\* Corresponding author at: Department of Physical and Environmental Sciences, University of Toronto Scarborough, 1265 Military Trail, Toronto, ON M1C 1A4, Canada. Tel.: +1 416 208 2786; fax: +1 416 287 7279.

E-mail address: [mdittrich@utsc.utoronto.ca](mailto:mdittrich@utsc.utoronto.ca) (M. Dittrich).

**Table 1**

Lake Sempach water column and sediment (at water depth of 87 m) characteristics.

Characteristics	Value <sup>a</sup>	Unit	Ref.	This study
Surface area	14.4	km <sup>2</sup>	Wieland et al. (1993)	
Volume	662 × 10 <sup>6</sup>	m <sup>3</sup>	Gächter and Imboden (1985)	
Maximum depth	87	m	Wieland et al. (1993)	
Hypolimnion flushing rate	0.09	yr <sup>-1</sup>	Wieland et al. (1993)	
Water retention time	17	yr	Urban et al. (1997)	
Solid sediment density	2.5	g cm <sup>-3</sup>		
Sedimentation flux	0.08	g cm <sup>-2</sup> yr <sup>-1</sup>	Furrer and Wehrli (1996)	
Average POC flux	620–873 (1988–1993)	μmol cm <sup>-2</sup> yr <sup>-1</sup>	Furrer and Wehrli (1996) Gächter and Meyer (1990)	
Average sedimentation flux of solid Mn	53 (1988–1993)	μmol cm <sup>-2</sup> yr <sup>-1</sup>	Gächter (unpublished)	5
Average sedimentation flux of solid Fe	30 (1988–1993)	μmol cm <sup>-2</sup> yr <sup>-1</sup>	Gächter (unpublished)	15
Average CaCO <sub>3</sub> flux	480 (1988–1993)	μmol cm <sup>-2</sup> yr <sup>-1</sup>	Muller et al. (2006)	420
O <sub>2</sub> in bottom water	>120 (>1984)	mmol/m <sup>3</sup>	Gächter and Stadelmann (1993)	
O <sub>2</sub> penetration depth	0.12–0.4	cm	Schauser et al. (2006) Muller et al. (2006)	0.3–1.0
O <sub>2</sub> consumption in sediment	0.31–0.58	mmol cm <sup>-2</sup> yr <sup>-1</sup>	Schauser et al. (2006); Urban et al. (1997) Muller et al. (2006)	0.5–1
P flux from sediment	1–10	μmol cm <sup>-2</sup> yr <sup>-1</sup>	Schauser et al. (2006) Urban et al. (1997)	2–7
Fe <sup>2+</sup> flux from sediment	0.7–24 (1989–1993)	μmol cm <sup>-2</sup> yr <sup>-1</sup>	Urban et al. (1997)	0–7
Mn <sup>2+</sup> flux from sediment	2.9–8.8 (1989–1993)	μmol cm <sup>-2</sup> yr <sup>-1</sup>	Urban et al. (1997)	1–8
NO <sub>3</sub> <sup>-</sup> flux into sediment	1–9 (1989–1993)	μmol cm <sup>-2</sup> yr <sup>-1</sup>	Urban et al. (1997)	8–16
% of P sedimentation flux released back to water	70		Schauser et al. (2006) Hupfer et al. (1995)	40–70
% of Fe sedimentation flux released back to water	15–27		Schauser et al. (2006)	0–40

<sup>a</sup> Dates in parentheses indicate years of measurements.

with a thermocline located between 5 and 15 m depth (Wieland et al., 1993). Until the 1950s, the lake was oligotrophic but subsequent increases in P loading lead to eutrophication and the lake's trophic status changed to mesotrophic around 1965 and to highly eutrophic by 1984 (Stadelmann, 1988). During 1965–1985, sewage discharge, extended use of phosphate detergents and high animal densities in agriculture contributed to the increase in total phosphorus concentration from 30 to 160 mg m<sup>-3</sup> (Fig. 1A; Buergi and Stadelmann, 2002). Starting in 1984, the hypolimnion was artificially aerated with oxygen in summer and the lake was artificially mixed between fall and spring every year (Stadelmann, 1988). At about the same time, external measures were implemented that decreased the nutrient inputs into the lake. As a result, P concentration decreased (Gächter and Wehrli, 1998) and the dissolved oxygen concentration in the hypolimnion increased to above 120 μmol L<sup>-1</sup> year-round. Starting from 1997, hypolimnion oxygenation with pure oxygen was replaced by aeration with fine air bubbles (Buergi and Stadelmann, 2002).

Low oxygen availability during the eutrophic period resulted in the absence of benthic bioturbation, and the sediment became laminated with no signs of mixing (Ambühl, 1994), seemingly down to the 1930s horizon (Buergi and Stadelmann, 2002). After the hypolimnion aeration, bioturbation resumed: sediment cores extracted from the deepest part of the lake in 1988 and 1994 contained a mixed surface layer (Wieland et al., 1993; Ambühl, 1994). Cores recovered by the present investigators from a water depth of 87 m in 2007 and 67 m in 2006 appeared bioturbated to a depth of 2–3 cm below the interface. Washing of the 2006 core revealed a small number of benthic organisms (about 20 per cm<sup>3</sup> of Tubificidae, Copepoda and Nematoda). Below the present depth of bioturbation, but clearly above the 1988–1994 horizons, the

sediment contained multiple distinct black layers, which likely formed due to episodic precipitation of iron sulfides in the previously bioturbated sediment.

The net sedimentation of phosphorus (defined as the difference between the sedimentation flux S and release flux R: S–R; Fig. 1B) calculated from a one-box mass balance model (Gächter and Meyer, 1993) indicated that the removal of phosphorus from the sediment was gradually increasing in the early stages of eutrophication (before 1967), likely following the increase in external P inputs. Between 1967 and 1977, however, the net sedimentation of phosphorus was decreasing despite the continuing increases in the external loadings and water column P concentrations. After 1984, phosphorus concentration in the water column decreased but the rate of phosphorus burial into the deep sediment remained relatively unchanged (Gächter and Muller, 2003). After 10 years of artificial oxygenation, Gächter and Wehrli (1998) attributed the decrease in the lake water phosphorus content to the reduction of the external P load, rather than to P retention in the sediment (Gächter and Wehrli, 1998). About 70% of the settled P was released back into the water column during early diagenesis (Hupfer et al., 1995; Schauser et al., 2006).

### 3. Methods

#### 3.1. Sampling and Fe extractions

Four replicate sediment cores were taken on November 27th, 2007 from a water depth of 87 m using a gravity corer (UWITEC) and Plexiglas core tubes 5.5 cm in diameter and ca. 70 cm in length. The cores were immediately brought to the laboratory and sectioned till 35 cm sediment depth under the N<sub>2</sub> atmosphere. Sub-samples

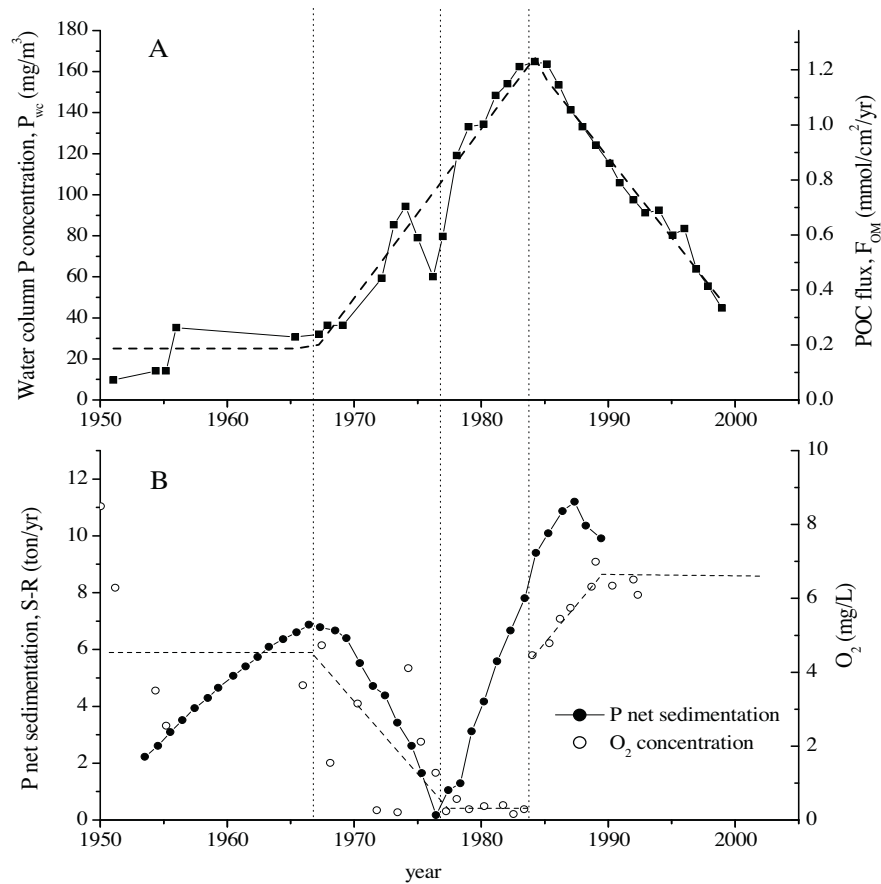


**Fig. 1.** (A) Total P concentration in the water column of Lake Sempach during spring overturn (Buergi and Stadelmann, 2002). The dashed line indicates our model's approximation for the sedimentation flux of particulate organic carbon. (B) Concentration of dissolved oxygen in the bottom water at fall overturn and the net (deposition minus release) sedimentation of phosphorus (Gächter and Stadelmann, 1993). The dashed line indicates our model's approximation of the SWI oxygen concentration.

of the obtained sections were placed in pre-weighted Petri dishes, freeze-dried for 60 h, and weighed again. The sediment water content was calculated based on the weight loss and used to estimate the porosity. The remaining sediment samples were analyzed for extractable iron according to the following protocol. The extractions distinguished three operationally defined iron pools (Poulton and Canfield, 2005; Tessier et al., 1979): loosely sorbed Fe (ascorbate extractable), Ca-bound Fe plus iron in acid volatile sulfides (AVS) (sodium acetate-extractable), and Fe-oxides. Approximately 1 g of wet sediment was extracted for 1 h with 10 mL of 1 M MgCl<sub>2</sub> pH 7 at room temperature by continuous shaking and centrifuging (Sorvall, Model RC2-B) at 10,000 rpm for 30 min. The supernatant was removed using a pipette and analyzed for Fe (see below), whereas the residue was washed in 8 mL of deionized water; after centrifugation for 30 min, the second supernatant was discarded. The volume of rinsed water used was kept to a minimum to avoid solubilization of solid material, particularly organic matter. The residue was extracted with 10 mL of 1 M sodium acetate NaOAc adjusted with acetic acid HOAc to pH 4.5 for 24 h at room temperature by continuous shaking and centrifuging at 10,000 rpm for 30 min. Again, the supernatant was removed with a pipette and analyzed for Fe (see below), whereas the residue was washed with 10 mL of deionized water; after centrifugation for 15 min, this supernatant was discarded. The third residue was extracted for 6 hours with 10 mL of dithionite in 25% acetic acid, 0.04 M NH<sub>2</sub>OH-HCl in 25% (v/v) HOAc at temperature  $96 \pm 2^\circ\text{C}$  (Tessier et al., 1979), discrete shaking and centrifuging at 10,000 rpm for 30 min. The supernatant was removed with a pipette and analyzed

for Fe content by an inductively coupled plasma-optical emission spectrometry (ICP-OES).

### 3.2. Burial velocity estimate

The burial velocity for sediment particles,  $U$  (cm yr<sup>-1</sup>), was calculated as a function of depth within the sediment,  $z$  (cm), as  $U = F / (1 - \varphi(z))\rho$ , where  $F$  is the sedimentation flux (in g cm<sup>-2</sup> yr<sup>-1</sup>),  $\rho = 2.5$  g cm<sup>-3</sup> is the density of dry sediment (e.g. Avnimelech et al., 2001) and  $\varphi(z)$  is the porosity. To approximate  $\varphi(z)$ , an analytical function (solid line in Fig. 2B) was fitted to measured porosity profiles. The porosity profiles in our 2007 cores and also 2004 cores (B. Müller, unpublished) were similar to the 1988 profile of Wieland et al. (1993), which suggests stationary compaction. The sedimentation flux  $F = 0.06$  g cm<sup>-2</sup> yr<sup>-1</sup> was chosen to match the sediment dating scale of previous works (M. Sturm, pers. comm). This value is slightly lower than the average value (0.067 g cm<sup>-2</sup> yr<sup>-1</sup>) measured in sediment traps in 1988–1993 (Gächter and Meyer, 1990; Wieland et al., 1993). The burial velocity decreases from about 0.5 cm yr<sup>-1</sup> at the sediment surface to 0.12 cm yr<sup>-1</sup> below 25 cm depth due to the sediment compaction (Fig. 2C).

### 3.3. Diagenetic modeling

Diagenetic modeling was performed using the diagenetic reaction-transport model LSSE-Mega, which is described in detail elsewhere (Katsev et al., 2006a, b, 2007). Briefly, the model solves a set of diagenetic equations for the concentrations  $C_i(x, t)$  of solid

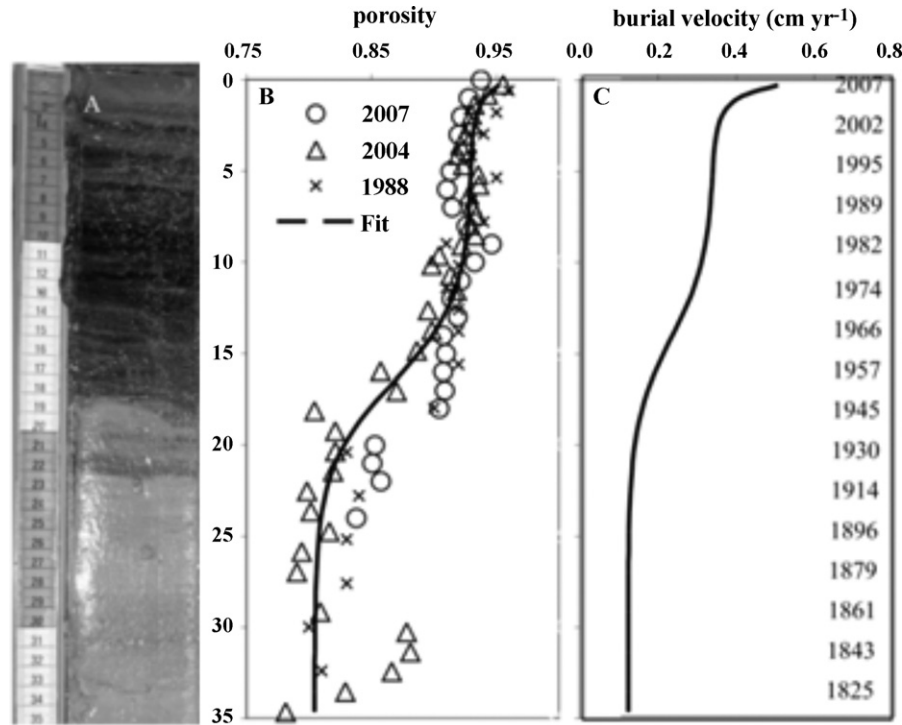


**Fig. 2.** (A) Lake Sempach sediment (November 2007; 87 m); (B) porosity in 2007 compared to the 2004 data (B. Müller, unpublished) and 1988 (Wieland et al., 1993). The solid line is the analytical fit used in the model; (C) Burial velocity.

(in mol per gram of dry weight (DW)) and dissolved (in mol cm<sup>-3</sup>) chemical species in the sediment:

$$\frac{\partial \xi C_i}{\partial t} = \frac{\partial}{\partial x} \left( \xi D_i \frac{\partial C_i}{\partial x} \right) - \frac{\partial}{\partial x} (\xi U_i C_i) + \sum_j \xi R_j(C_i) \quad (1)$$

Here,  $t$  is time and  $x$  is the depth coordinate from the sediment–water interface down.  $U_i$  is the advection (burial) velocity. The factor  $\xi$  is equal to the sediment porosity  $\phi$  for dissolved species and  $(1 - \phi)\rho$  for solid species, where  $\rho$  is the grain density of dry sediment in g cm<sup>-3</sup>. The effective diffusion coefficients  $D_i$  were calculated as sums of the bioturbation coefficient  $D_b$  and the appropriate molecular diffusion coefficients  $D_{diff}^{sed}$ , which were calculated based on the molecular diffusion coefficients  $D_{diff}$  corrected for sediment porosity  $\phi$  using Archie's law and for temperature  $T$  using expressions in Boudreau (1997) for  $T = 5^\circ\text{C}$ .

$$D_{diff}^{sed} = \frac{D_{diff}}{1 - \ln(\phi^2)} \quad (2)$$

The depth dependence of the bioturbation coefficient,  $D_b(x)$ , is approximated by

$$D_b = D_b^0 \frac{1 - \tanh(x - H)/\tau_b}{1 - \tanh(-H/\tau_b)} \quad (3)$$

where  $D_b^0$  is the value at the sediment surface,  $H$  is the depth of the steepest gradient of  $D_b(x)$  within the sediment and  $\tau_b = 1.43$  cm is the characteristic depth half-interval within which most of the decrease in  $D_b$  occurs (Table 2; Katsev et al., 2006b).

Microbial decomposition of organic matter (OM) (represented by a nominal composition  $(\text{CH}_2\text{O})_x(\text{NH}_3)_y(\text{H}_3\text{PO}_4)_z$  in reactions (1)–(4); Table 2) is described by the Michaelis–Menten kinetics (Fig. 3; Katsev et al., 2006b; Boudreau, 1997). The rate constants for the rates  $R_j$  of chemical and biochemical reactions (Fig. 3) are shown in Tables 3 and 4.

Reversible sorption of the ferrous iron ion on sediment solid surfaces is described by a pH-dependent equilibrium partitioning coefficient  $K_{adsFe}$  approximated by a Langmuir isotherm:

$$[\text{ads-Fe}] = K_{adsFe} [\text{Fe}^{2+}] \quad (4)$$

where

$$K_{adsFe} = \sum \frac{K_{Fe,i}^* X_i S_{Ti}}{[\text{H}^+] + K_{Fe,i}^* [\text{Fe}^{2+}]} \quad (5)$$

Here, square brackets denote the concentrations of the respective species and the sum runs over two types of solid substrates: ferric oxyhydroxides ( $\text{Fe}(\text{OH})_3$ ), and a “background” (B) which collectively represents all other sediment solids. Ferric oxyhydroxides are singled out because of their high specific sorption capacity for phosphate (Parfitt, 1989) and their susceptibility to redox-driven dissolution/precipitation that are central to the classical model of phosphorus release (Boström et al., 1988).  $[\text{ads-Fe}]$  is the concentration of adsorbed Fe (in mol/gDW),  $X_i$  is the weight fraction of the  $i$ -th adsorption substrate ( $i = 1, 2$ ),  $S_{Ti}$  is the density (in mol/gDW) of sorption sites at the substrate surface.

The constants  $K_{Fe,i}^*$  (Table 3) characterize specific sorption capacities of the substrates. The term  $[\text{H}^+]$  accounts for the pH-driven increase in  $K_{adsFe}$  within a pH interval roughly extending from 5 to 7. By analogy, the adsorption coefficient for phosphate  $K_{adsP}$  is defined as

$$[\text{ads-P}] = K_{adsP} [\text{P}_{diss}] \quad (6)$$

where

$$K_{adsP} = \sum \frac{K_{P,i}^* X_i S_{Ti}}{[\text{OH}^-] + K_{P,i}^* [\text{P}_{diss}]} \quad (7)$$

Here,  $[\text{P}_{diss}]$  is the aqueous total (all ionic species combined) phosphate concentration (in mol cm<sup>-3</sup>) and  $[\text{ads-P}]$  is the concentration of adsorbed phosphate (in mol g<sup>-1</sup> DW). The coefficients  $S_{Ti}$  and  $K_{P,i}^*$  for the Fe(III) substrate were obtained (Katsev et al., 2006b) by

**Table 2**

Model reactions. ‘S–X’ denotes adsorption of a species X to a site S– on a solid substrate;  $R'$  denote dissolution rates. Total analytical variables ([TC], [TS], and [ALK], respectively) were used to characterize the aqueous concentrations of porewater carbonate, sulfide, and alkalinity: [TC] =  $[\text{CO}_3^{2-}] + [\text{HCO}_3^-] + [\text{CO}_3^{2-}]$ , [TS] =  $[\text{HS}^-] + [\text{H}_2\text{S}]$  and [ALK] =  $[\text{HCO}_3^-] + [\text{CO}_3^{2-}] + [\text{HS}^-] - [\text{NH}_4^+] + \text{F}[\text{ads-Fe}] - [\text{H}^+] + [\text{OH}^-]$ .

Kinetic reactions	Rates	Reaction number
<b>Primary redox reactions</b>		
$(\text{CH}_2\text{O})(\text{NH}_3)_y(\text{H}_3\text{PO}_4)_z + (1 + 2y)\text{O}_2 + y\text{HCO}_3^- \rightarrow (1 + y)\text{CO}_2 + y\text{NO}_3^- + z\text{H}_3\text{PO}_4 + (1 + y)\text{H}_2\text{O}$	$R_{\text{O}_2}$	1
$(\text{CH}_2\text{O})(\text{NH}_3)_y(\text{H}_3\text{PO}_4)_z + 4/5\text{NO}_3^- \rightarrow 1/5\text{CO}_2 + 4/5\text{HCO}_3^- + 2/5\text{N}_2 + y\text{NH}_3 + z\text{H}_3\text{PO}_4 + 3/5\text{H}_2\text{O}$	$R_{\text{NO}_3}$	2
$(\text{CH}_2\text{O})(\text{NH}_3)_y(\text{H}_3\text{PO}_4)_z + 2\text{MnO}_2 + (3 + y)\text{CO}_2 + (1 + y)\text{H}_2\text{O} \rightarrow 2\text{Mn}^{2+} + (4 + y)\text{HCO}_3^- + y\text{NH}_4^+ + z\text{H}_3\text{PO}_4$	$R_{\text{MnO}_2}$	3
$(\text{CH}_2\text{O})(\text{NH}_3)_y(\text{H}_3\text{PO}_4)_z + 4\text{Fe}(\text{OH})_3 + 7\text{CO}_2 \rightarrow 4\text{Fe}^{2+} + 8\text{HCO}_3^- + y\text{NH}_3 + z\text{H}_3\text{PO}_4 + 3\text{H}_2\text{O}$	$R_{\text{Fe}(\text{OH})_3}$	4
$(\text{CH}_2\text{O})(\text{NH}_3)_y(\text{H}_3\text{PO}_4)_z + 1/2\text{SO}_4^{2-} \rightarrow \text{HCO}_3^- + 1/2\text{H}_2\text{S} + y\text{NH}_3 + z\text{H}_3\text{PO}_4$	$R_{\text{SO}_4}$	5
$(\text{CH}_2\text{O})(\text{NH}_3)_y(\text{H}_3\text{PO}_4)_z \rightarrow 1/2\text{CH}_4 + 1/2\text{CO}_2 + y\text{NH}_3 + z\text{H}_3\text{PO}_4$	$R_{\text{CH}_4}$	6
<b>Secondary redox reactions</b>		
$4\text{Fe}^{2+} + \text{O}_2 + 8\text{HCO}_3^- + 2\text{H}_2\text{O} \rightarrow 4\text{Fe}(\text{OH})_3 + 8\text{CO}_2$	$R_{\text{FeO}_x}$	7
$4\text{S}^- \text{Fe}^+ + \text{O}_2 + 4\text{HCO}_3^- + 6\text{H}_2\text{O} \rightarrow 4\text{S}^- \text{H}^0 + 4\text{Fe}(\text{OH})_3 + 4\text{CO}_2$	$R_{\text{surFe}}$	8
$\text{S}^- \text{Mn}^+ + 1/2\text{O}_2 + \text{HCO}_3^- \rightarrow \text{S}^- \text{H}^0 + \text{MnO}_2 + \text{CO}_2$	$R_{\text{surMn}}$	9
$\text{NH}_4^+ + 2\text{O}_2 + 2\text{HCO}_3^- \rightarrow \text{NO}_3^- + 2\text{CO}_2 + 3\text{H}_2\text{O}$	$R_{\text{NH}_4\text{O}_x}$	10
$\text{H}_2\text{S} + 2\text{O}_2 + 2\text{HCO}_3^- \rightarrow \text{SO}_4^{2-} + 2\text{CO}_2 + 2\text{H}_2\text{O}$	$R_{\text{SO}_x}$	11
$\text{FeS} + 2\text{O}_2 \rightarrow \text{Fe}^{2+} + \text{SO}_4^{2-}$	$R_{\text{FeSO}_x}$	12
$2\text{FeS}_2 + 9\text{O}_2 + 5\text{H}_2\text{O} \rightarrow 2\text{Fe}(\text{OH})_3 + 4\text{SO}_4^{2-} + 4\text{H}^+$	$R_{\text{FeS}_2\text{O}_x}$	13
$2\text{Fe}^{2+} + \text{MnO}_2 + 4\text{H}_2\text{O} \rightarrow 2\text{Fe}(\text{OH})_3 + \text{Mn}^{2+} + 2\text{H}^+$	$R_{\text{FeMnO}_2}$	14
$\text{MnO}_2 + \text{HS}^- + 3\text{H}^+ \rightarrow \text{Mn}^{2+} + \text{S}^0 + 2\text{H}_2\text{O}$	$R_{\text{MnO}_2\text{S}}$	15
$4\text{MnO}_2 + \text{NH}_4^+ + 6\text{H}^+ \rightarrow 4\text{Mn}^{2+} + \text{NO}_3^- + 5\text{H}_2\text{O}$	$R_{\text{MnNH}_4}$	16
$5\text{Mn}^{2+} + 2\text{NO}_3^- + 4\text{H}_2\text{O} \rightarrow 5\text{MnO}_2 + \text{N}_2 + 8\text{H}^+$	$R_{\text{MnNO}_3}$	17
$2\text{Fe}(\text{OH})_3 + \text{H}_2\text{S} + 4\text{CO}_2 \rightarrow 2\text{Fe}^{2+} + \text{S}^0 + 4\text{HCO}_3^- + 2\text{H}_2\text{O}$	$R_{\text{SFe}_3}$	18
$\text{Fe}_3(\text{PO}_4)_2 + 3\text{H}_2\text{S} \rightarrow 3\text{FeS} + 2\text{H}_3\text{PO}_4$	$R_{\text{Sviv}}$	19
$\text{FeCO}_3 + \text{H}_2\text{S} \rightarrow \text{FeS} + \text{CO}_2 + \text{H}_2\text{O}$	$R_{\text{SFeCO}_3}$	20
$\text{FeS} + \text{H}_2\text{S} \rightarrow \text{FeS}_2 + \text{H}_2$	$R_{\text{FeSHS}}$	21
$\text{FeS} + \text{S}^0 \rightarrow \text{FeS}_2$	$R_{\text{pyr}}/R_{\text{pyr}}$	22
$4\text{S}^0 + 4\text{H}_2\text{O} \rightarrow \text{SO}_4^{2-} + 3\text{HS}^- + 5\text{H}^+$	$R_{\text{S}^0\text{disp}}$	23
<b>Mineral precipitation reactions</b>		
$\text{Fe}^{2+} + \text{HCO}_3^- + \text{HS}^- \leftrightarrow \text{FeS} + \text{CO}_2 + \text{H}_2\text{O}$	$R_{\text{FeS}}/R'_{\text{FeS}}$	24
$3\text{Fe}^{2+} + 2\text{H}_3\text{PO}_4 \leftrightarrow \text{Fe}_3(\text{PO}_4)_2 + 6\text{H}^+$	$R_{\text{viv}}/R'_{\text{viv}}$	25
$a\text{Fe}^{2+} + (1 - a)\text{Ca}^{2+} + 2\text{HCO}_3^- \leftrightarrow \text{Fe}_a\text{Ca}_{1-a}\text{CO}_3 + \text{CO}_2 + \text{H}_2\text{O} (a = 1)$	$R_{\text{FeCO}_3}/R'_{\text{FeCO}_3}$	26
$b\text{Mn}^{2+} + (1 - b)\text{Ca}^{2+} + 2\text{HCO}_3^- \leftrightarrow \text{Mn}_b\text{Ca}_{1-b}\text{CO}_3 + \text{CO}_2 + \text{H}_2\text{O} (b = 0.95)$	$R_{\text{MnCO}_3}/R'_{\text{MnCO}_3}$	27
$\text{Ca}^{2+} + \text{CO}_3^{2-} \leftrightarrow \text{CaCO}_3$	$R_{\text{CaCO}_3}/R'_{\text{CaCO}_3}$	28
<b>Local equilibrium reactions</b>		
<i>Adsorption</i>		
$\text{H}_3\text{PO}_4 \leftrightarrow \text{H}_3\text{PO}_4(\text{ads})$	$K_{\text{adsP}}$	29
$\text{S}^- \text{H}^0 + \text{Fe}^{2+} + \text{HCO}_3^- \leftrightarrow \text{S}^- \text{Fe}^+ + \text{CO}_2 + \text{H}_2\text{O}$	$K_{\text{adsMn}}$	30
$\text{S}^- \text{H}^0 + \text{Mn}^{2+} + \text{HCO}_3^- \leftrightarrow \text{S}^- \text{Mn}^+ + \text{CO}_2 + \text{H}_2\text{O}$	$K_{\text{adsFe}}$	31
$\text{NH}_4^+ \leftrightarrow \text{NH}_4^+(\text{ads})$	$K_{\text{adsNH}_4}$	32
$\text{NH}_3 \leftrightarrow \text{NH}_3(\text{ads})$	$K_{\text{adsNH}_3}$	33
<i>Acid–base reactions</i>		
$\text{CO}_2(\text{aq}) + \text{H}_2\text{O} \leftrightarrow \text{HCO}_3^- + \text{H}^+$	$K_{\text{C1}} = [\text{H}^+][\text{HCO}_3^-]/[\text{CO}_2]$	34
$\text{HCO}_3^- \leftrightarrow \text{CO}_3^{2-} + \text{H}^+$	$K_{\text{C2}} = [\text{H}^+][\text{CO}_3^{2-}]/[\text{HCO}_3^-]$	35
$\text{NH}_4^+ \leftrightarrow \text{NH}_3 + \text{H}^+$	$K_{\text{NH}} = [\text{H}^+][\text{NH}_3]/[\text{NH}_4^+]$	36
$\text{H}_2\text{S} \leftrightarrow \text{HS}^- + \text{H}^+$	$K_{\text{HS}} = [\text{H}^+][\text{HS}^-]/[\text{H}_2\text{S}]$	37
$\text{H}_2\text{O} \leftrightarrow \text{H}^+ + \text{OH}^-$	$K_{\text{W}} = [\text{H}^+][\text{OH}^-]$	38

fitting the experimental data of Parfitt (1989) for phosphate sorption on goethite ( $\alpha\text{-FeOOH}$ ). In the previous study of (Katsev et al., 2006b), the choice of the sorption isotherm had an insignificant effect on the magnitude of phosphorus efflux from the sediment.

The boundary conditions at the sediment–water interface are fixed-concentration (Dirichlet) for the dissolved species:

$$C_i(x = 0, t) = C_i^0(t) \quad (8)$$

and fixed-flux (Neumann) for the solid species:

$$-\xi D_i \frac{\partial C_i}{\partial x} + \xi U_i C = F_i(t) \quad (9)$$

Here,  $F_i$  is the solid substance flux (in  $\text{mol cm}^{-2} \text{yr}^{-1}$ ) at the sediment–water interface. A no-gradient boundary condition is imposed for all species at the bottom of the integration domain:

$$\frac{\partial C_i}{\partial x_{x=L}} = 0. \quad (10)$$

Sediment compaction was calculated from a measured porosity profile (as described in Katsev et al., 2007). Solid-phase calcium

carbonate and dissolved ionic calcium were considered explicitly (see Tables 2–4 for model reactions, kinetic law formulations, and best-fit parameters).

For lack of sediment geochemistry data prior to 1960s, we calibrated the model first at steady state using an extensive data set collected in Lake Sempach between 1988 and 1994. The sedimentation flux of organic carbon,  $F_{\text{OM}}$  and the interface oxygen concentration,  $[\text{O}_2]^0$ , were then adjusted to match the pre-eutrophic conditions of 1967, and the model was again run to a steady state. The model was then propagated forward in time using the time-dependent boundary conditions as shown in Fig. 1. The SWI oxygen concentration was approximated by the measured bottom water  $\text{O}_2$  concentration (Gächter and Stadelmann, 1993; Muller and Stadelmann, 2004) (Fig. 1B). The flux of degradable organic matter (Fig. 1A), was taken as proportional to the concentration of phosphorus in the water column (Buerger and Stadelmann, 2002) with a coefficient of proportionality 0.007 estimated from the sediment trap data (Furrer and Wehrli, 1996; Wehrli and Wüest, 1996). The sedimentation fluxes of reactive and refractory (or non-degradable) organic matter,  $F_{\text{OM1}}$  and  $F_{\text{OM2}}$ , respectively, were

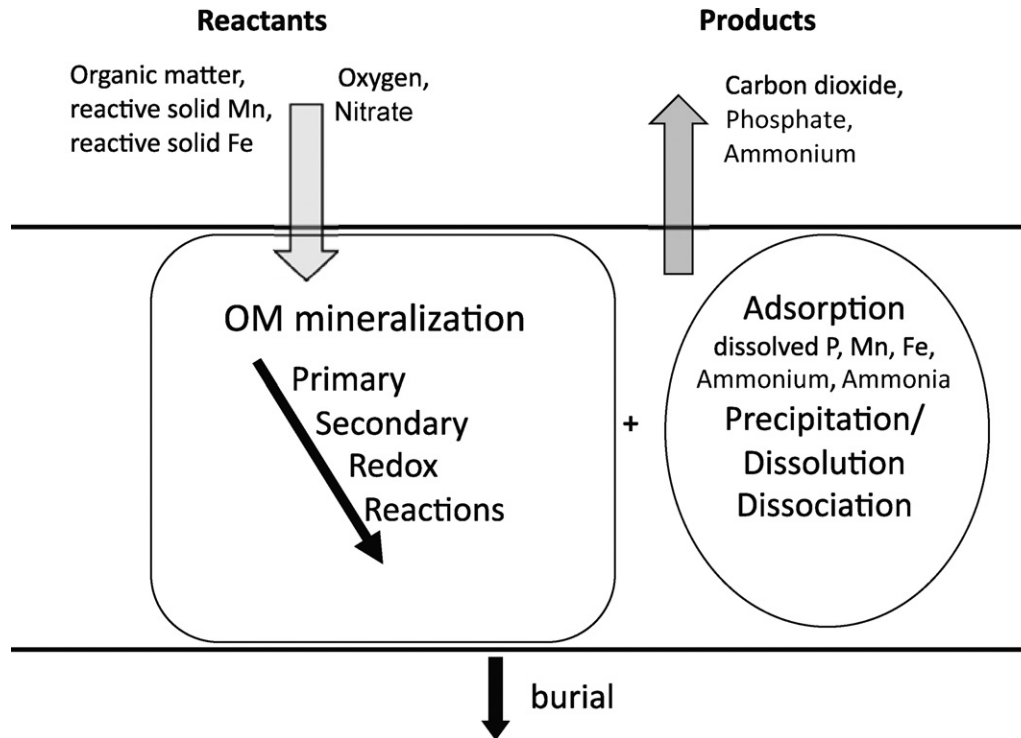


**Fig. 3.** A conceptual diagram of the diagenetic model for solid and dissolved components. Organic matter represented by a nominal composition  $\text{CH}_2\text{O}_x(\text{NH}_3)_y(\text{H}_3\text{PO}_4)_z$  is decomposed by microorganisms via a cascade of electron acceptors (Berg et al., 2003). The model includes variety of geochemical reactions such as adsorption, precipitation/dissolution, acid–base dissociations.

considered as fixed fractions of the total flux,  $F_{\text{OM}}$ . For lack of time-resolved historical data, the model considered sedimentation fluxes of Fe and Mn as being constant in time and neglected transport from littoral to profundal areas of the lake (Urban et al., 1997). To account for the effect of oxygen depletion on benthic macrofauna, the bioturbation coefficient,  $D_b^0$ , was varied with the SWI oxygen concentration as described by the non-threshold approximation (Katsev et al., 2007). This had only a minor effect in our simulations because the bioturbation rates in Lake Sempach are low. Bioirrigation was neglected because of the absence of bioirrigating organisms.

## 4. Results

### 4.1. Iron fractionation

The sediment distribution of the dithionite-extractable iron exhibited a minimum between 8 and 20 cm depth (Fig. 4). The concentrations of the acetate-extractable iron are correspondingly higher in this depth range (Fig. 4), indicating that, upon the reduction of iron oxides, the mobilized iron precipitated as sulfides; the presence of sulfides is evidenced by the black color of the sediment core within this depth interval. A similar pattern – a decreased concentration of dithionite-extractable iron in black sediment layers – was also observed in another core extracted from 65 m water depth in 2006 (not shown).

### 4.2. Simulation results

The model was successful at capturing the main features of chemical distributions within the sediment (Fig. 5). Discrepancies between the simulated and measured depth distributions of sediment solids and solutes are attributed to factors such as strong seasonal variability, dependence of the sediment composition on

its previous history, and uncertainties in model parameterizations. The largest uncertainty is associated with the lack of information about the initial, pre-eutrophic, state and the time evolutions of such parameters as the sedimentation fluxes of reactive iron and manganese (Dittrich et al., 2009).

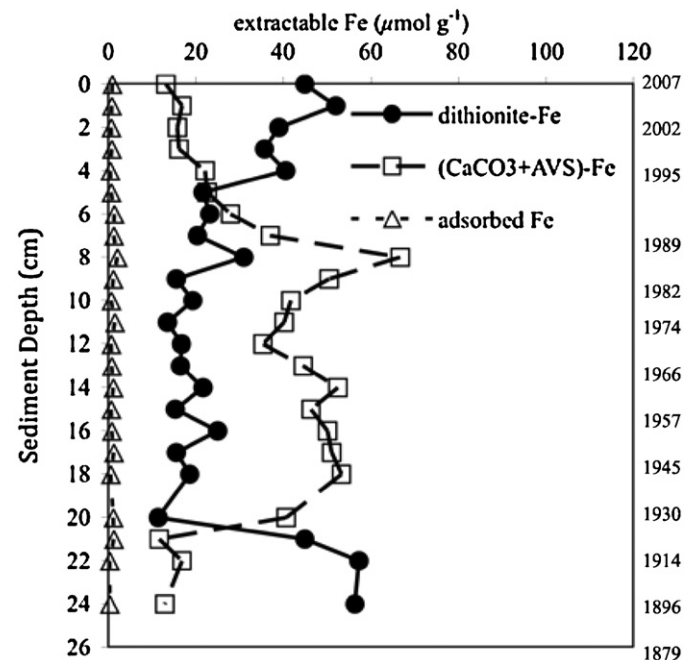


**Fig. 4.** Iron fractions in a sediment core extracted in November 2007 from 87 m depth. Three sequentially extractable iron fractions: loosely sorbed Fe (ascorbate extractable), Ca-bound Fe plus iron in acid volatile sulfides (AVS) (sodium acetate-extractable), and reactive reducible Fe (dithionite extractable).

**Table 3**  
Model rates.

Reactions	Rates
Primary redox reactions For $i, j = (\text{O}_2, \text{NO}_3, \text{MnO}_2, \text{Fe}(\text{OH})_3, \text{SO}_4)$	$R_i = (k_{\text{OM1}}[\text{OM1}] + k_{\text{OM2}}[\text{OM2}])f_i$ , where $f_i = \frac{C_i}{C_i + C_i^{\text{lim}}} \prod_{j=1}^{i-1} \frac{C_j^{\text{lim}}}{C_j + C_j^{\text{lim}}} \cdot f_{\text{CH}_4} = 1 - \sum_{j=1}^5 f_j$
Secondary redox reactions	$R_{\text{FeO}_x} = k_{\text{FeO}_x}[\text{Fe}^{2+}][\text{O}_2]$ $R_{\text{surFe}} = k_{\text{surFe}}[\text{ads-Fe}][\text{O}_2]$ $R_{\text{NH}_4\text{O}_x} = k_{\text{NH}_4\text{O}_x}[\text{TN}][\text{O}_2]$ , where $[\text{TN}] = [\text{NH}_4^+] + [\text{NH}_3]$ $R_{\text{SO}_x} = k_{\text{SO}_x}[\text{TS}][\text{O}_2]$ , where $[\text{TS}] = [\text{H}_2\text{S}] + [\text{HS}^-]$ $R_{\text{FeSO}_x} = k_{\text{FeSO}_x}[\text{FeS}][\text{O}_2]$ $R_{\text{FeS}_2\text{O}_x} = k_{\text{FeS}_2\text{O}_x}[\text{FeS}_2][\text{O}_2]$ $R_{\text{FeMnO}_2} = k_{\text{FeMnO}_2}[\text{Fe}^{2+}][\text{MnO}_2]$ $R_{\text{MnO}_2\text{S}} = k_{\text{MnO}_2\text{S}}[\text{MnO}_2][\text{TS}]$ $R_{\text{MnNH}_4} = k_{\text{MnNH}_4}[\text{MnO}_2][\text{TN}]$ $R_{\text{MnNO}_3} = k_{\text{MnNO}_3}[\text{Mn}^{2+}][\text{NO}_3^-]$ $R_{\text{SFe}_3} = k_{\text{SFe}_3}[\text{TS}][\text{Fe}(\text{OH})_3]$ $R_{\text{Sviv}} = k_{\text{Sviv}}[\text{TS}][\text{Fe}_3(\text{PO}_4)_2]$ $R_{\text{SFeCO}_3} = k_{\text{SFeCO}_3}[\text{TS}][\text{FeCO}_3]$ $R_{\text{FSHS}} = k_{\text{FSHS}}[\text{FeS}][\text{TS}]$ $R_{\text{pyr}} = k_{\text{pyr}}[\text{FeS}][\text{S}^0]$ ; $R'_{\text{pyr}} = k'_{\text{pyr}}[\text{FeS}_2]$ $R_{\text{S}^0\text{disp}} = k_{\text{S}^0\text{disp}}[\text{S}^0]$
Mineral precipitation reactions	<p>(Here, <math>H(x) = 1</math> for <math>x &gt; 0</math> and <math>H(x) = 0</math> for <math>x \leq 0</math>)</p> $R_{\text{FeS}} = k_{\text{FeS}}(\Omega_{\text{FeS}} - 1)H(\Omega_{\text{FeS}} - 1)$ $R'_{\text{FeS}} = k'_{\text{FeS}}[\text{FeS}](1 - \Omega_{\text{FeS}})H(1 - \Omega_{\text{FeS}})$ where $\Omega_{\text{FeS}} = \frac{[\text{Fe}^{2+}][\text{HS}^-]}{K_{\text{FeS}}[\text{H}^+]}$ and $[\text{HS}^-] = \frac{[\text{TS}]}{1 + [\text{H}^+]/K_{\text{HS}}}$ $R_{\text{viv}} = k_{\text{viv}}(\Omega_{\text{viv}}^\alpha - 1)H(\Omega_{\text{viv}}^\alpha - 1)$ $R'_{\text{viv}} = k'_{\text{viv}}[\text{Fe}_3(\text{PO}_4)_2]_2(1 - \Omega_{\text{viv}}^\alpha)H(1 - \Omega_{\text{viv}}^\alpha)$ where $\Omega_{\text{viv}} = \frac{[\text{Fe}^{2+}]^3[\text{P}_{\text{diss}}]^2}{k_{\text{viv}}}$ and $\alpha = 1/5$ $R_{\text{FeCO}_3} = k_{\text{FeCO}_3}(\Omega_{\text{FeCO}_3} - 1)H(\Omega_{\text{FeCO}_3} - 1)$ $R'_{\text{FeCO}_3} = k'_{\text{FeCO}_3}[\text{FeCO}_3](1 - \Omega_{\text{FeCO}_3})H(1 - \Omega_{\text{FeCO}_3})$ where $\Omega_{\text{FeCO}_3} = \frac{[\text{Fe}^{2+}][\text{CO}_3^{2-}]}{aK'_{\text{FeCO}_3}}$ and $[\text{CO}_3^{2-}] = \frac{[\text{TC}]}{1 + [\text{H}^+]/K_{\text{C2}} + [\text{H}^+]^2/K_{\text{C1}}K_{\text{C2}}}$ $R_{\text{MnCO}_3} = k_{\text{MnCO}_3}(\Omega_{\text{MnCO}_3} - 1)H(\Omega_{\text{MnCO}_3} - 1)$ $R'_{\text{MnCO}_3} = k'_{\text{MnCO}_3}[\text{MnCO}_3](1 - \Omega_{\text{MnCO}_3})H(1 - \Omega_{\text{MnCO}_3})$ where $\Omega_{\text{MnCO}_3} = \frac{[\text{Mn}^{2+}][\text{CO}_3^{2-}]}{bK'_{\text{MnCO}_3}}$ $R_{\text{CaCO}_3} = k_{\text{CaCO}_3}(\Omega_{\text{CaCO}_3} - 1)H(\Omega_{\text{CaCO}_3} - 1)$ $R'_{\text{CaCO}_3} = k'_{\text{CaCO}_3}[\text{CaCO}_3](1 - \Omega_{\text{CaCO}_3})H(1 - \Omega_{\text{CaCO}_3})$ , where $\Omega_{\text{CaCO}_3} = \frac{[\text{Ca}^{2+}][\text{CO}_3^{2-}]}{K'_{\text{CaCO}_3}}$

#### 4.2.1. Organic carbon mineralization pathways

Simulations suggest that, prior to 1967, oxygen concentrations were high, organic carbon fluxes were low and more than half of the deposited organic matter was mineralized by oxic respiration (Fig. 6). Subsequent increases in organic carbon loading resulted in the increased overall rate of carbon mineralization ( $\text{CO}_2$  production). As oxygen levels declined, oxic respiration was replaced by alternative mineralization pathways (see Table 2 for modeled reactions). As mineralization by solid-phase electron acceptors (Mn and Fe oxides) was limited by their available amounts, the contributions of Mn reduction and Fe reduction to carbon mineralization were small, in the order of a few percent of the total  $\text{CO}_2$  production. In contrast to marine sediments where aerobic respiration is typically replaced by sulfate reduction (Morse and Eldridge, 2007), the rate of sulfate reduction was comparable to the rates of iron and manganese reductions. Under low-oxygen conditions, aerobic respiration was therefore replaced predominantly by methanogenesis (Furrer and Wehrli, 1996). In the mid-1980s, methanogenesis may have accounted for more than 60% of the organic carbon mineralization (Fig. 6B). As methanogenesis is typically slower than the more energetic mineralization pathways, whereas in the model the total mineralization rate is pathway-independent, refractory organic matter may have been accumulating in the sediment during the period of low-oxygen conditions. After the organic matter sedimentation flux decreased in the mid-1980s (Fig. 1) and oxic conditions were restored, the relative contribution of oxic respiration increased. Our simulations suggest that, at present, up to 50%

of the deposited organic carbon is mineralized aerobically near the sediment–water interface (Fig. 6), which compares favorably with the 28% estimated by and the 50% estimated by previous studies (Muller et al., 2003, 2006).

#### 4.2.2. Changes in sediment composition

During the eutrophic period, the increased OC sedimentation had increased the concentration of particulate organic carbon (POC) below the SWI (Fig. 5). The reverse process was observed after the restoration measures in the mid-1980s. Sediment concentrations of solid manganese and iron oxides declined in response to decreasing oxygen levels at the onset of eutrophication. Reductive dissolution of the Fe oxides by the freshly deposited organic matter resulted in a trough in the solid-Fe profile below the depths of oxygen penetration and Mn reduction (Figs. 2 and 6). The mobilized Fe(II) precipitated near the oxic–anoxic boundary, generating a Fe(III)-enrichment there. As the sediment porewater contained hydrogen sulfide generated by sulfate reduction, some of the reduced iron precipitated as sulfide FeS (Dittrich et al., 2009). The reduced Mn in the solid phase remained mostly in the form of Mn carbonates (Friedl et al., 1997). Sediment concentration of solid calcium carbonate remained relatively unaltered. The lake receives large amounts of detrital calcite (Muller et al., 2006) but we have no information about the temporal changes in the calcite input from the catchment.

Changes in the concentrations of dissolved species in the sediment pore water were comparable in magnitude to their

**Table 4**  
Model parameters.

Parameter	Value	Units	Literature values	Refs.
Simulated sediment depth ( $L$ )	30	cm		
Solid sediment density ( $\rho$ )	2.5	$\text{g cm}^{-3}$		
Burial velocity at depth ( $L$ , $U_L$ )	0.15	$\text{cm yr}^{-1}$		
N:C ratio in OM ( $y$ )	0.143	$\text{g g}^{-1}$		
P:C ratio in OM ( $z$ )	0.02	$\text{g g}^{-1}$	0.01–0.02	Hecky et al. (1993), Gächter (unpublished), Urban et al. (1997), Hupfer et al. (1995)
Bioturbation coeff. at surface ( $D_b^0$ )	2.0	$\text{cm}^2 \text{yr}^{-1}$	0.1–5	Katsev and Dittrich (unpublished), Francois et al. (2002), Matisoff et al. (1999), Katsev et al. (2004)
Depth of max. bioturbation gradient ( $H$ )	0	cm		
Bioturbation depth attenuation ( $\tau_b$ )	1.43	cm	1–3	Wieland et al. (1993)
$[\text{O}_2]^0$	$1.2 \times 10^{-7}$	$\text{mol cm}^{-3}$	$(1.0\text{--}2.1) \times 10^{-7}$	Gächter (unpublished), Gächter and Stadelmann (1993), Muller et al. (2006)
$[\text{NO}_3]^0$	$1.0 \times 10^{-8}$	$\text{mol cm}^{-3}$	$(1\text{--}3) \times 10^{-8}$	Gächter (unpublished), Urban et al. (1997)
$[\text{SO}_4]^0$	$1.0 \times 10^{-7}$	$\text{mol cm}^{-3}$	$(0.5\text{--}1.5) \times 10^{-7}$	Gächter (unpublished), Urban et al. (1997)
$[\text{TC}]^0$	$2.87 \times 10^{-6}$	$\text{mol cm}^{-3}$	$(1.5\text{--}3.0) \times 10^{-6}$	Gächter (unpublished), Muller et al. (2006)
$[\text{ALK}]^0$	$2.73 \times 10^{-6}$	$\text{mol cm}^{-3}$		Gächter (unpublished)
$[\text{Ca}^{2+}]^0$	$1.3 \times 10^{-6}$	$\text{mol cm}^{-3}$	$(1.0\text{--}1.3) \times 10^{-6}$	Gächter (unpublished), Muller et al. (2006)
$[\text{Fe}^{2+}]^0$	$1.0 \times 10^{-9}$	$\text{mol cm}^{-3}$		Gächter (unpublished), Urban et al. (1997)
$[\text{Mn}^{2+}]^0$	$1.0 \times 10^{-9}$	$\text{mol cm}^{-3}$		Gächter (unpublished), Urban et al. (1997)
$[\text{H}_3\text{PO}_4]^0$	$6 \times 10^{-7}$	$\text{mol cm}^{-3}$		Gächter (unpublished)
Flux of reactive OM ( $F_{\text{OM1}}$ )	$1.14 \times 10^{-4}$	$\text{mol cm}^{-2} \text{yr}^{-1}$	$<6 \times 10^{-4}$	Gächter (unpublished), 5, 24
Flux of weakly reactive OM ( $F_{\text{OM2}}$ )	$0.4 \times 10^{-4}$	$\text{mol cm}^{-2} \text{yr}^{-1}$	$<6 \times 10^{-4}$	Gächter (unpublished), Furrer and Wehrli (1996), Gächter and Meyer (1990)
Flux of refractory OM, no decay OM	$1.3 \times 10^{-4}$	$\text{mol cm}^{-2} \text{yr}^{-1}$	$<6 \times 10^{-4}$	Gächter (unpublished), Furrer and Wehrli (1996), Gächter and Meyer (1990)
Flux of reactive Fe(III) ( $F_{\text{Fe(OH)}_3}$ )	$1.5 \times 10^{-5}$	$\text{mol cm}^{-2} \text{yr}^{-1}$	$<3 \times 10^{-5}$	Gächter (unpublished)
Flux of reactive Mn oxide ( $F_{\text{MnO}_2}$ )	$0.5 \times 10^{-5}$	$\text{mol cm}^{-2} \text{yr}^{-1}$	$<5 \times 10^{-5}$	Gächter (unpublished)
Reactivity of OM1 ( $k_{\text{OM1}}$ )	2.0	$\text{yr}^{-1}$		
Reactivity of OM2 ( $k_{\text{OM2}}$ )	0.05	$\text{yr}^{-1}$		
Monod constant ( $C_{\text{O}_2}^{\text{lim}}$ )	$2.0 \times 10^{-9}$	$\text{mol cm}^{-3}$	$10^{-10}$ to $10^{-8}$	Van Cappellen and Wang (1996)
Monod constant ( $C_{\text{NO}_3}^{\text{lim}}$ )	$2.0 \times 10^{-7}$	$\text{mol cm}^{-3}$	$(2\text{--}80) \times 10^{-9}$	Berg et al. (2003)
Monod constant ( $C_{\text{MnO}_2}^{\text{lim}}$ )	$2.0 \times 10^{-4}$	$\text{mol g}^{-1}$		
Monod constant ( $C_{\text{Fe(OH)}_3}^{\text{lim}}$ )	$2.0 \times 10^{-3}$	$\text{mol g}^{-1}$	$(0.3\text{--}10) \times 10^{-5}$	Schauser et al. (2004), Roden and Wetzel (2002), Ferro (2003)
Monod constant ( $C_{\text{SO}_4}^{\text{lim}}$ )	$7.0 \times 10^{-7}$	$\text{mol cm}^{-3}$	$(0.6\text{--}10) \times 10^{-7}$	Van Cappellen and Wang (1996), Pallud and Van Cappellen (2006), Schauser et al. (2004)
$k_{\text{FeOx}}$	$0.35 \times 10^{11}$	$\text{cm}^3 \text{mol}^{-1} \text{yr}^{-1}$		Katsev et al. (2006a, b), Van Cappellen and Wang (1996)
$k_{\text{SurFe}}$	$1.25 \times 10^{10}$	$\text{cm}^3 \text{mol}^{-1} \text{yr}^{-1}$		Katsev et al. (2006a, b)
$k_{\text{NH}_4\text{Ox}}$	$5 \times 10^9$	$\text{cm}^3 \text{mol}^{-1} \text{yr}^{-1}$	$5 \times 10^9$	Katsev et al. (2007), Van Cappellen and Wang (1996)
$k_{\text{SO}_4}$	$1.6 \times 10^{10}$	$\text{cm}^3 \text{mol}^{-1} \text{yr}^{-1}$	$>1.6 \times 10^8$	Katsev et al. (2007), Van Cappellen and Wang (1996)
$k_{\text{FeSO}_4}$	$1.0 \times 10^9$	$\text{cm}^3 \text{mol}^{-1} \text{yr}^{-1}$	$10^8\text{--}10^{10}$	Katsev et al. (2007), Hunter et al. (1998)
$k_{\text{FeS}_2\text{Ox}}$	$2 \times 10^8$	$\text{cm}^3 \text{mol}^{-1} \text{yr}^{-1}$	$10^8$	Katsev et al. (2007), Wijsman et al. (2002)
$k_{\text{FeMnO}_2}$	$3.0 \times 10^9$	$\text{cm}^3 \text{mol}^{-1} \text{yr}^{-1}$	$10^6\text{--}3 \times 10^9$	Van Cappellen and Wang (1996), Berg et al. (2003), Stumm and Morgan (1996)
$k_{\text{MnO}_2\text{S}}$	$2.0 \times 10^7$	$\text{cm}^3 \text{mol}^{-1} \text{yr}^{-1}$	$(1\text{--}2) \times 10^7$	Van Cappellen and Wang (1996), Katsev et al. (2007), Hunter et al. (1998)
$k_{\text{MnNH}_4}$	0	$\text{cm}^3 \text{mol}^{-1} \text{yr}^{-1}$		
$k_{\text{MnNO}_3}$	0	$\text{cm}^3 \text{mol}^{-1} \text{yr}^{-1}$		
$k_{\text{SFe}_3}$	$4 \times 10^6$	$\text{cm}^3 \text{mol}^{-1} \text{yr}^{-1}$	$10^4\text{--}10^8$	Katsev et al. (2006a, b), Hunter et al. (1998), Wijsman et al. (2002)
$k_{\text{Sviv}}$	$1.0 \times 10^8$	$\text{cm}^3 \text{mol}^{-1} \text{yr}^{-1}$	$(01\text{--}1) \times 10^8$	Katsev et al. (2006a, b, 2007)
$k_{\text{SFeCO}_3}$	$1.0 \times 10^7$	$\text{cm}^3 \text{mol}^{-1} \text{yr}^{-1}$	$(1\text{--}5) \times 10^7$	Katsev et al. (2006a, b, 2007)
$k_{\text{SFESH}}$	$1.0 \times 10^3$	$\text{cm}^3 \text{mol}^{-1} \text{yr}^{-1}$		
$k_{\text{pyr}}$	$1.0 \times 10^5$	$\text{g mol}^{-1} \text{yr}^{-1}$		Katsev et al. (2007)
$k'_{\text{pyr}}$	0.01	$\text{yr}^{-1}$		Katsev et al. (2007)
$k_{\text{S}^0\text{disp}}$	0.12	$\text{yr}^{-1}$		Katsev et al. (2007)
$k_{\text{FeS}}$	$1 \times 10^{-6}$	$\text{mol g}^{-1} \text{yr}^{-1}$	$10^{-7}$ to $10^{-4}$	Van Cappellen and Wang (1996), Katsev et al. (2006a, b)
$k'_{\text{FeS}}$	$1.0 \times 10^{-3}$	$\text{yr}^{-1}$		Van Cappellen and Wang (1996), Katsev et al. (2007)
$K_{\text{FeS}}$	$2.51 \times 10^{-6}$	$\text{mol cm}^{-3}$		Katsev et al. (2007), Morse and Cornwell (1987), Morse et al. (1987)
$k_{\text{FeCO}_3}$	$6.5 \times 10^{-4}$	$\text{mol g}^{-1} \text{yr}^{-1}$		
$k'_{\text{FeCO}_3}$	0.05	$\text{yr}^{-1}$		
$K'_{\text{FeCO}_3}$	$3.98 \times 10^{-13}$	$(\text{mol cm}^{-3})^2$		
$k_{\text{MnCO}_3}$	$1 \times 10^{-5}$	$\text{mol g}^{-1} \text{yr}^{-1}$	$(1\text{--}100) \times 10^{-4}$	Van Cappellen and Wang (1996), Katsev et al. (2007)
$k'_{\text{MnCO}_3}$	0.25	$\text{yr}^{-1}$	$10^{-2}$ to $10^3$	Van Cappellen and Wang (1996), Katsev et al. (2007)
$K'_{\text{MnCO}_3}$	$2.2 \times 10^{-14}$	$(\text{mol cm}^{-3})^2$		
$k_{\text{CaCO}_3}$	$1.0 \times 10^{-5}$	$\text{mol g}^{-1} \text{yr}^{-1}$		
$k'_{\text{CaCO}_3}$	0.05	$\text{yr}^{-1}$		
$K'_{\text{CaCO}_3}$	$1.9 \times 10^{-15}$	$(\text{mol cm}^{-3})^2$		
$k_{\text{viv}}$	$1.0 \times 10^{-10}$	$\text{mol g}^{-1} \text{yr}^{-1}$		Katsev et al. (2007)
$k'_{\text{viv}}$	1.0	$\text{yr}^{-1}$		Katsev et al. (2007)
$K_{\text{viv}}$	$3.0 \times 10^{-50}$	$(\text{mol cm}^{-3})^5$		Katsev et al. (2007), Davison (1993)

Table 4 (Continued)

Parameter	Value	Units	Literature values	Refs.
<i>Equilibrium adsorption parameters</i>				
$K'_{\text{FeonFe}}$	$5 \times 10^{-4}$	–	$<2 \times 10^{-3}$	Dzombak and Morel (1990)
$K'_{\text{FeonMn}}$	$1 \times 10^{-5}$	–	$<2 \times 10^{-3}$	Dzombak and Morel (1990)
$K'_{\text{FeonB}}$	$2.0 \times 10^{-1}$	–		
$K'_{\text{MnonFe}}$	$2 \times 10^{-5}$	–		
$K'_{\text{MnonMn}}$	$1 \times 10^{-5}$	–		
$K'_{\text{MnonB}}$	$2 \times 10^{-5}$	–		
$K'_{\text{PonFe}}$	$2.0 \times 10^{-4}$	–	$<2 \times 10^{-3}$	Dzombak and Morel (1990)
$K'_{\text{PonB}}$	$0.2 \times 10^{-6}$	–		
$K_{\text{adsNH}_4}, K_{\text{adsNH}_3}$	1.4	–		Van Cappellen and Wang (1996)
$S_{\text{TFe}}, S_{\text{TMn}}$	$1.0 \times 10^{-2}$	$\text{mol g}^{-1}$		Katsev et al. (2007)
$S_{\text{TB}}$	$3.0 \times 10^{-5}$	$\text{mol g}^{-1}$		Katsev et al. (2007)

Definitions of the model parameters can be found in Katsev et al. (2007). Interface concentrations (for solutes) and sedimentation fluxes (for solids) not listed in this table are zero.  $[\text{O}_2]^0$  and OM flux values are specified for the calibration steady state.

respective seasonal variations (Fig. 5). The simulations suggest that, at the onset of low-oxygen conditions, the gradients of the pore water nitrate and sulfate steepened in the vicinity of the interface, whereas their concentrations in the sediment pore water decreased. Contrary to the suggestion of Furrer and Wehrli (1996) that the pH in Lake Sempach is controlled solely by the dissolution of calcium carbonate, we find that the pore water pH is significantly affected by the reduction of iron and sulfate. When iron and sulfate reduction was turned off in the model, the simulated pH profile was consistently lower than the measured values. Our simulations suggest that sulfate reduction increased the pH by about 1 unit across a wide depth range within the sediment, whereas iron reduction was responsible for a small pH increase of around  $x=2$  cm (Fig. 6).

#### 4.2.3. Fluxes across the sediment–water interface

At the onset of eutrophic conditions at the beginning of the 1970s, the increased rates of Mn reduction generated an increased flux of Mn(II) from the sediment (Fig. 7) until the reactive Mn oxide pool near the sediment–water interface became nearly exhausted (around 1971; Fig. 7). At that point, Fe oxides became utilized for organic carbon mineralization, generating a flux of Fe(II) from the sediment. The Mn efflux then increased slightly for the second time, as some of the reduced Fe(II) was re-oxidized by the remaining Mn oxides. Restoration of oxic conditions in 1984 sharply decreased the Fe efflux (Fig. 7). The Fe(II) flux continued to decrease gradually in the following years, as the thickness of the oxidized sediment layer increased (Schäuser et al., 2006). Phosphorus effluxes decreased briefly when the aeration caused precipitation of Fe(III) oxides, but it subsequently returned to the relatively high values because the amount of oxidized iron was yet insufficient to adsorb enough P from the pore water.

The effect of elemental fluxes from the sediment on the sediment pools of Fe, Mn, and P may be illustrated using the mass-balance principle. Fig. 8 shows the fluxes of Mn, Fe, and P from the diagenetically active part of the sediment (upper 30 cm), both up into the water column and down into the deep sediment (due to the burial of the solid sediment and pore water). The shown fluxes are normalized to the total sedimentation fluxes of the respective species; thus during the times where the sum of the two fluxes exceeded 1, the diagenetically active layer was being depleted of the respective element, whereas the element accumulated when the sum of the two fluxes was smaller than 1. During the eutrophic period, the sediment was being strongly depleted in Mn and somewhat depleted in Fe (Fig. 8). At the peak of eutrophication in the early 1980s, more than 90% of the deposited Mn and about 25% of the deposited Fe were being returned to the water column. Deposition of phosphorus during the years of peak loadings resulted in both higher effluxes of phosphorus into the water column and P accumulation in the sediment (Fig. 8). Restoration thus improved both phosphorus retention within the diagenetically active surface

sediment layer and phosphorus burial into the inactive deeper layers.

Simulations suggest that the effects of dissolved sulfate and hydrogen sulfide on P mobilization were minor (Roden and Edmonds, 1997). The dissolution of vivianite (iron phosphate,  $\text{Fe}_3(\text{PO}_4)_2 \cdot 8(\text{H}_2\text{O})$ ) by hydrogen sulfide was not important because of the relatively small amount of vivianite. The removal of Fe(II) from active circulation by its precipitation as FeS had only minor effects.

## 5. Discussion

### 5.1. Phosphorus cycling and mobilization mechanisms

Increases in phosphorus fluxes from sediment may come either from the increased deposition and recycling of phosphorus, or from a remobilization of the previously accumulated phosphorus pool. That between 1967 and 1977 the rate of phosphorus release from the sediment,  $R$ , was increasing faster than the rate of phosphorus deposition,  $S$  (Fig. 1b), implies a mobilization of the previously accumulated phosphorus during that period. We hypothesize that the mobilization of previously accumulated phosphorus was caused by the loss of the sediment ferric iron pool. This is supported by the minimum in the distribution of dithionite-extractable iron and the corresponding accumulation of acetate-extractable iron (Fig. 4), which suggest that declining oxygen levels (Fig. 1b) at the onset of eutrophication resulted in the conversion of Fe oxides into the reduced Fe forms. Similarly, a brief increase in  $(S-R)$  after the restoration of oxic conditions in 1984 can be attributed, at least in part, to a re-accumulation of the Fe(III) oxides within the sediment. Comparison of Figs. 2 and 4 indicates that the concentrations of Fe oxides in the Lake Sempach sediments began to increase around 1984, i.e. after the beginning of the hypolimnion aeration.

Simulations and field measurements indicate that about 66% of the deposited phosphorus is mobilized in the upper 10 cm, i.e. within 20 years of deposition (Urban et al., 1997; Hupfer et al., 1995). Most of the mobilized phosphate becomes bound to iron oxyhydroxides. This iron-bound phosphorus, however, is not removed from active circulation and becomes remobilized when iron oxides dissolve in the reduced sediment within 5–10 years of their deposition (Fig. 4; Hupfer et al., 1995). Only about 17% of the phosphorus being buried into the deep sediment is associated with inorganic substrates. Simulations suggest that P is removed from active circulation primarily by burial with refractory organic fractions. To not be released into the water column, the mobilized phosphorus must be either incorporated in stable mineral phases within the reduced sediment (an unlikely P sink in sulfidic Lake Sempach sediments), or accumulate in the diagenetically active surface sediment layer. As the continuously eutrophic conditions in Lake Sempach resulted in the Fe(III) mineral surfaces within the

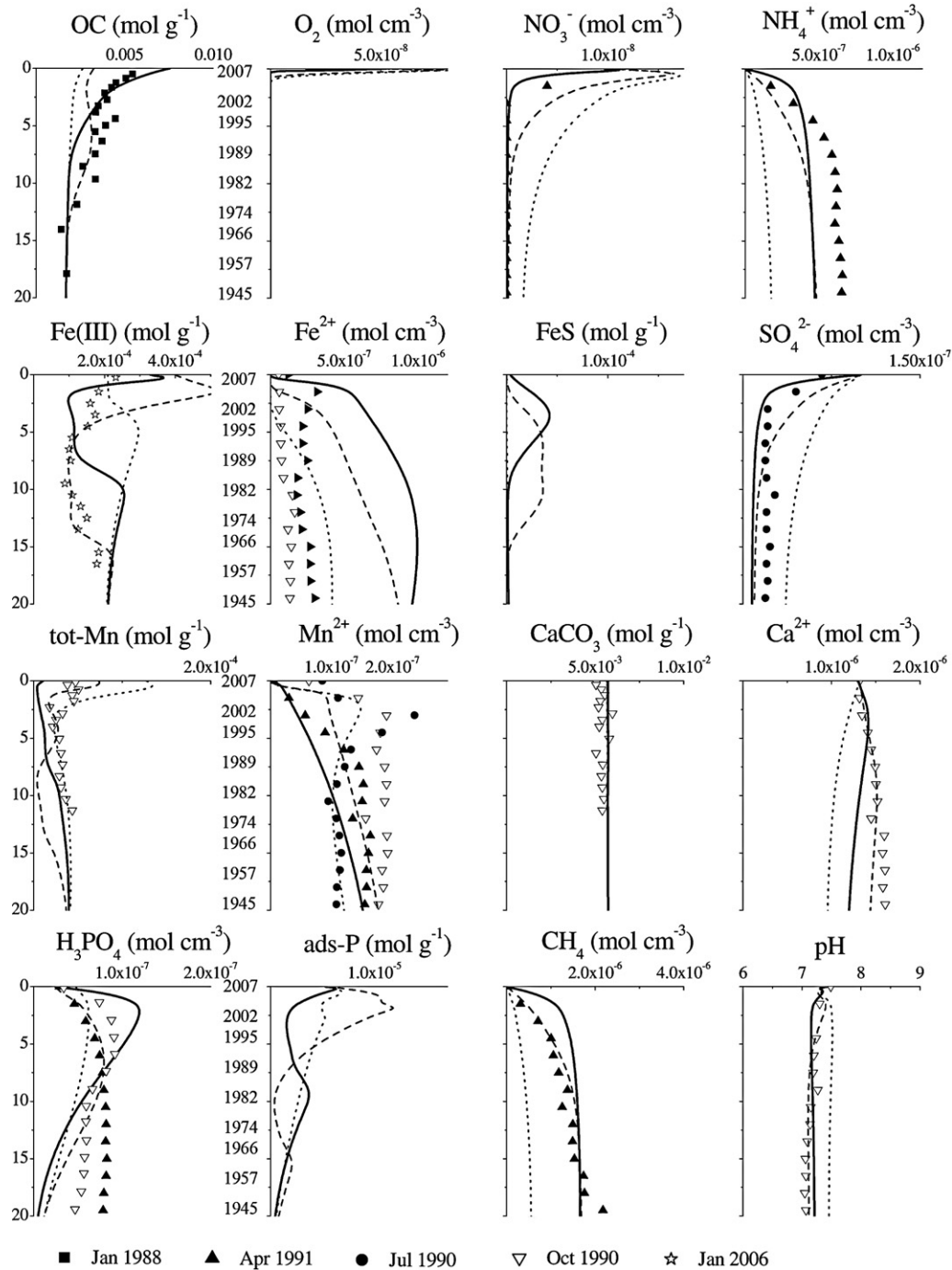


**Fig. 5.** Model solutions for the pre-eutrophic steady state (dotted), 1984 (solid), and 2006 (dashed). Representative geochemical data (symbols) for 80–87 m depth are from Höhener and Gächter (1993), Furrer and Wehrli (1996), Urban et al. (1997), Müller et al. (2006), Gächter (unpublished), and Müller (unpublished).

diagenetically active layer being saturated with phosphorus (Hupfer et al., 2000, 1995), the sediment binding capacity for phosphorus could only increase with the size of the Fe(III) pool. An order-of-magnitude calculation suggests that, upon the restoration of oxic conditions, the resultant increase in the size of sediment Fe(III) pool could decrease the P efflux by about  $4.5 \mu\text{mol cm}^{-2} \text{yr}^{-1}$ , which is comparable to the P flux due to the decomposition of organic matter (about  $4 \mu\text{mol cm}^{-2} \text{yr}^{-1}$ ) and to the observed P effluxes (Table 1). Similarly, at the beginning of eutrophication, increases in P effluxes of similar magnitude could be potentially generated by the dissolution of Fe(III) oxides, which could take place over 20 years from the initial concentration of  $0.1 \text{ mmol g}^{-1}$ .

Our simulations suggest, however, that the variations in the sediment Fe(III) pool and their contributions to P effluxes were smaller.

The dynamics of phosphorus evolution in the sediments of Lake Sempach thus can be recapped as follows. Prior to around 1967, increases in the external phosphorus inputs were mitigated by the available sediment sorption capacity: phosphorus accumulated in the near-surface sediment layer, increasing the P:Fe ratio. The flux of reactive organic matter was likely low enough to support only limited Fe reduction. If the meso-trophic conditions of that period persisted, the adsorbed phosphorus could have been eventually buried into the deep sediment with Fe(III) solids. In particular, if the artificial oxygenation of the lake's hypolimnion started between

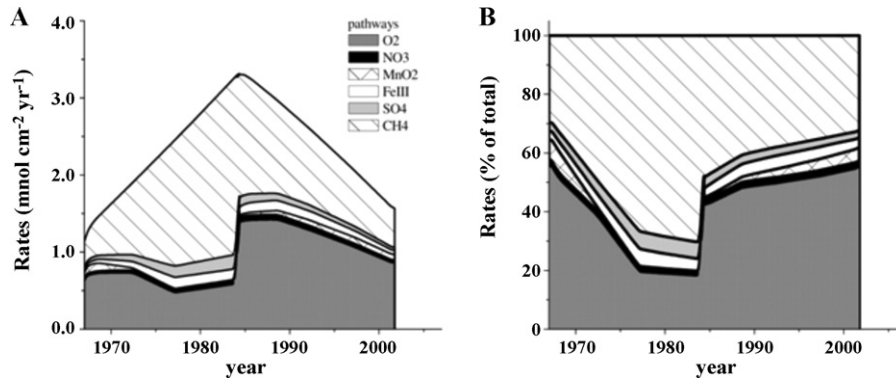


Fig. 6. Rates of organic matter mineralization pathways integrated over the top 30 cm of sediment. (A) Absolute values; (B) normalized to the total rate of  $\text{CO}_2$  production.

1967 and 1977, i.e. when the sediment Fe(III) pool was not being depleted, it could have been effective in improving the P retention (Figs. 1 and 9). After the sediment Fe(III) pool was depleted, the sediment phosphorus content and, ultimately, the efflux of phosphorus into the water column were not controlled by the rate of P burial into the deep sediment but by P sedimentation. As the P effluxes reflected P mobilization from labile organic particles, the phosphorus effluxes rose and fell with organic sedimentation fluxes (Figs. 1 and 8). Most of the released phosphorus was being returned to the sediment with organic sedimentation at the end of the season, hence on an annual basis the water column P concentrations followed the trends in the external loadings of phosphorus to the lake, even though the external loading was smaller than the internal one (Gächter and Wehrli, 1998).

The restoration measures in 1984 reversed the process. Currently, redox conditions at the sediment surface are similar to those during the pre-eutrophic period, and a large fraction of the presently deposited ferric iron is expected not to be immobilized in the reduced sediment for lack of reductant. When the deposited P is being permanently buried with the Fe(III) phases, artificial oxygenation of the lake hypolimnion may be discontinued.

Fig. 9 shows that the relationship between the net phosphorus sedimentation ( $S-R$ ) and the water column P content,  $P_{\text{WC}}$ , exhibited a hysteresis. The regions with a negative slope of ( $S-R$ ) vs.  $P_{\text{WC}}$  curve correspond to the times where the sediment retention of phosphorus was being affected by the sediment Fe(III) content. Phosphorus retention during those periods was sensitive to the redox conditions and oxygen levels. Regions of positive slope indicate the times when the retention of phosphorus followed organic sedimentation and was insensitive to the sediment redox regime.

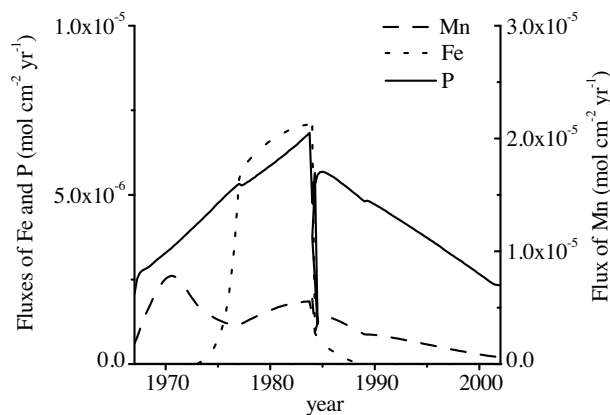


Fig. 7. Fluxes of Fe(II), Mn(II), and phosphate from sediment into the water column.

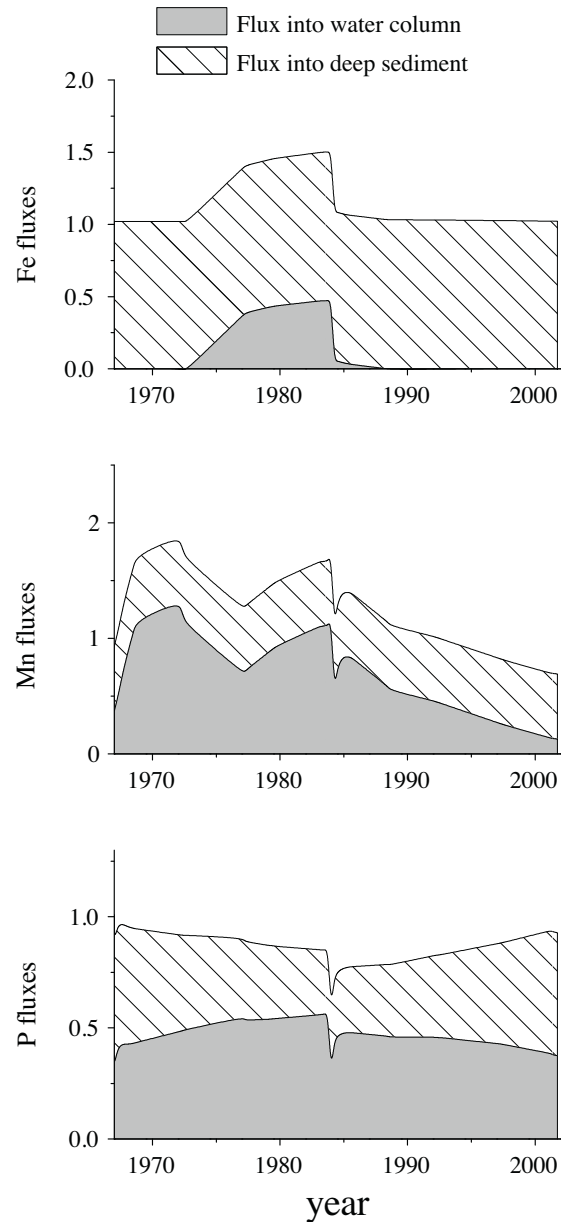
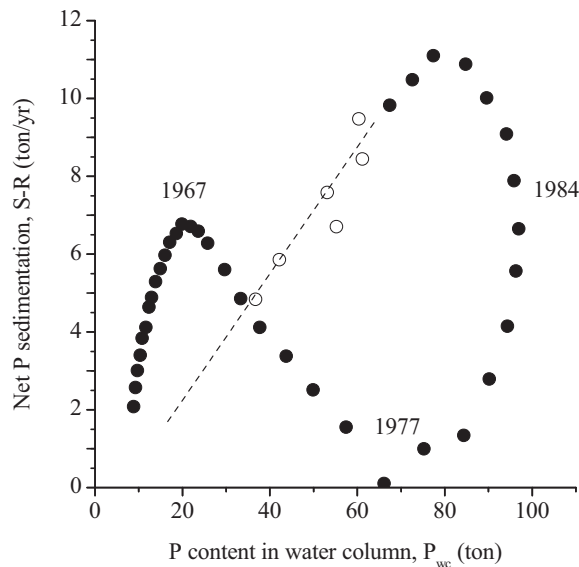


Fig. 8. Fluxes of P, Fe and Mn from the diagenetically active layer into the water column and into the deep (>30 cm) sediment. The fluxes are normalized to the total sedimentation fluxes of the respective elements. Sum values smaller than 1 indicate the net accumulation of the element within the top 30 cm of sediment, whereas values greater than 1 indicate depletion.



**Fig. 9.** A hysteresis-type relationship between the net phosphorus sedimentation ( $S-R$ ) and P concentration in the water column,  $P_{wc}$ . Filled symbols are from Gächter and Stadelmann (1993). Open symbols are the output from our sediment model. The regions of negative slope (1967–1977 and 1984–1988) likely reflect the time periods when sediment phosphorus retention was most affected by the redox-sensitive cycle of sediment iron.

### 5.2. Phosphorus mass balance in the water column

The predicted phosphorus effluxes can be verified against the historical record of water column P concentrations using a mass balance model (Gächter and Imboden, 1985):

$$V \frac{dP_{wc}}{dt} = I - O - (S - R) \quad (11)$$

Here,  $I$  is the rate of input of phosphorus from all sources into the lake,  $O$  is the rate of P removal with the outflow,  $S$  is the sedimentation rate of phosphorus and  $R$  is the rate of phosphorus release from the sediments;  $V$  is the lake volume (Table 1). This model provides an internal consistency check for the sediment–water column coupling, as the sediment model considered the sedimentation

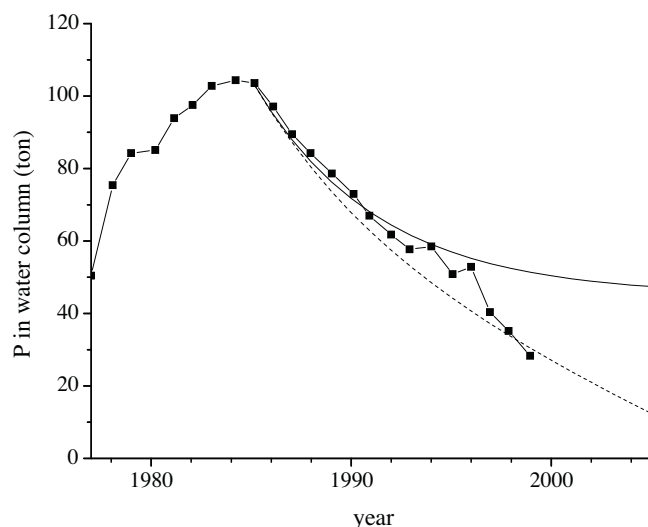


**Fig. 10.** Phosphorus content in the water column calculated from the mass balance model (Eq. (11)) assuming constant (solid) and decreasing (dashed) external inputs of phosphorus ( $I$ ). The net phosphorus sedimentation ( $S-R$ ) was taken from the sediment model.

flux of phosphorus as a fixed (Redfield-type) fraction of the sedimentation flux of organic matter. Following Gächter and Wehrli (1998), we first assumed a constant external phosphorus input,  $I = 7 \text{ tons yr}^{-1}$ , and a phosphorus outflow rate,  $O$  ( $\text{tons yr}^{-1}$ ), proportional to the water column P concentration (tons):  $O = 0.09P_{wc}$  (Eq. (11)). Fig. 10 shows the solution for  $P_{wc}$  that was obtained when the net phosphorus sedimentation ( $S-R$ ) was approximated by the output from our sediment model. The net sedimentation of phosphorus, ( $S-R$ ), decreases concomitant with the decrease in  $S$  after 1984 (Fig. 10). The  $P_{wc}$  reaches an approximately constant level at about  $50 \mu\text{mol L}^{-1}$ . This agrees with previous predictions (Wehrli and Wüest, 1996) but disagrees with observations (Fig. 10). The continuous decline in  $P_{wc}$  that was observed is therefore likely due to the reduction in the external P input, which was implemented as part of the lake remediation measures (Gächter and Wehrli, 1998). A dotted line shows the model solution for which the P input was assumed to decrease as  $I(t) = 7 - 0.2t$ . When the decrease in the external input is taken into account, the simulations agree with the observations, suggesting that the sediment–water column coupling is internally consistent. We therefore conclude that, in Lake Sempach, the decrease in the lake water phosphorus content over the past 20 years resulted mainly from the reduction in the external P inputs (Gächter and Wehrli, 1998).

## 6. Conclusions

### 6.1. What controls phosphorus retention in lake sediments?

Mobilization of phosphorus in aquatic sediments is often described using a so-called ‘classical Fe–P model’ (Einsele, 1936; Mortimer, 1941), which was remarkably successful in describing seasonal phosphorus releases in a variety of environments (Boström et al., 1988). According to this model, phosphorus availability is controlled by the redox conditions in the uppermost sediment layer. At the onset of anoxic conditions, iron oxyhydroxides at the sediment surface are reductively dissolved and the phosphate that had been adsorbed by them is released into the sediment pore water, from where it diffuses into the overlying water. In recent decades, numerous deviations from the classical model were reported: anoxia did not always cause phosphorus release and oxic conditions did not necessarily prevent P mobilization (Caraco et al., 1991; Gächter and Müller, 2003). Some of the proposed alternative mechanisms of phosphorus mobilization focused on the processes near the sediment–water interface: hydrogen sulfide, for example, was suggested to mobilize phosphorus by directly dissolving Fe(III) solids (Caraco et al., 1989; Roden and Edmonds, 1997), and in Lake Sempach an insufficiently thick oxidized layer was suggested as a reason for poor P retention (Gächter and Wehrli, 1998). Another group of hypotheses concentrated on phosphorus retention in the deep sediment. For example, the failure of hypolimnetic oxygenation to decrease phosphorus effluxes in Lake Sempach was suggested to have resulted from poor permanent burial of P (Hupfer et al., 1995; Schauser et al., 2006). Hydrogen sulfide was hypothesized to prevent phosphate immobilization with ferrous solids by binding dissolved Fe(II) as FeS (Caraco et al., 1989; Roden and Edmonds, 1997), as well as by directly dissolving phosphorus-bearing ferrous minerals such as vivianite (Gächter and Müller, 2003).

Alternatively to the focus on P mobilization mechanisms, a time scale argument (Katsev et al., 2006b) suggests that the near-interface processes may be considered as responsible for the short-term behaviors, such as seasonal P releases, whereas processes that affect P burial into the deep sediment determine the sediment P effluxes on decadal and longer time scales. The decadal scale of most lake restoration projects is intermediate between

the seasonal time scale and the time scale on which sediment processes achieve a steady state (Katsev et al., 2006a, b). For this reason, short-term approaches such as those of the classical model (Mortimer, 1941), and steady state models (Schäuser et al., 2006) alike may provide only limited insights. Sensitivity analyses (e.g. Katsev et al., 2006b) consistently reveal that the long-term sediment P effluxes are primarily sensitive to the sedimentation flux of organic matter (Dittrich et al., 2009) and secondarily to the SWI oxygen concentrations. As oxygen levels affect phosphorus fluxes over the time scale of the sediment iron cycle (several years), dissolved oxygen should not be considered as the factor that controls P mobility in the long term. In fact, even in the short term, the key characteristic is not the O<sub>2</sub> concentration but the balance between the supply rates of oxygen and its organic reductants (e.g. Katsev et al., 2006a; Li et al., 2012), as iron is reduced and phosphorus is released when the flux of organic matter exceeds the mineralization capacity of oxic respiration. Over the long term, however, the focus of the phosphorus-controlling restoration measures should be on restricting the external P inputs into the lake.

## Acknowledgments

We acknowledge financial support from the Swiss National Science Foundation (SNF Nr 200021-107985/1). S.K. was supported by the postdoctoral fellowship from the Natural Science and Engineering Research Council of Canada (NSERC) and by the University of Minnesota Duluth start-up funds. M.D. was supported by the Connaught Fund (University of Toronto). We thank Sabine Sibling for her help with chemical extractions, Michael Schuler for the sampling, Doris Hohmann for enumeration of benthic community, Beat Müller and René Gächter for sharing data.

## References

- Ambühl, H., 1994. Die Feinstruktur jüngster Sedimente von Seen verschiedenen Trophiegrades und von Seen mit technischer Sanierung. *Limnologische Berichte Donau* 2, 1011–1238.
- Avnimelech, Y., Ritvo, G., Meijer, L.E., Kochba, M., 2001. Water content, organic carbon and dry bulk density in flooded sediments. *Aquacultural Engineering* 25, 25–33.
- Berg, P., Rysgaard, S., Thamdrup, B., 2003. Dynamic modeling of early diagenesis and nutrient cycling. A case study in an Arctic marine sediment. *American Journal of Science* 303, 905–955.
- Boström, B., Andersen, J.M., Fleischer, S., Jansson, M., 1988. Exchange of phosphorus across the sediment–water interface. *Hydrobiologia* 170, 229–244.
- Boström, B., Jansson, M., Forsberg, C., 1982. Phosphorus release from lake sediments. *Archiv für Hydrobiologie – Beiheft Ergebnisse der Limnologie* 18, 5–59.
- Boudreau, B.P., 1997. *Diagenetic Models and their Implementation*. Springer.
- Buergi, H., Stadelmann, P., 2002. Change of phytoplankton composition and biodiversity in Lake Sempach before and during restoration. *Hydrobiologia* 469, 33–48.
- Burdige, D.J., 2006. *Geochemistry of Marine Sediments*. Princeton University Press, Princeton.
- Caraco, N.F., Cole, J.J., Likens, G.E., 1989. Evidence for sulphate-controlled phosphorus release from sediments of aquatic systems. *Letters to Nature* 341, 316–318.
- Caraco, N.F., Cole, J.J., Likens, G.E., 1991. Phosphorus release from anoxic sediments—lakes that break the rules. *International Association of Theoretical and Applied Limnology – Proceedings* 24 (Pt 5), 2985–2988.
- Davison, W., 1993. Iron and manganese in lakes. *Earth Science Reviews* 34, 119–163.
- Dittrich, M., Wehrli, B., Reichert, P., 2009. Lake sediments during the transient eutrophication period: reactive-transport model and identifiability study. *Ecological Modelling* 220, 2751–2769.
- Dzombak, D.A., Morel, F.M.M., 1990. *Surface Complexation Modeling: Hydrous Ferric Oxide*. Wiley-Interscience, New York, 393 p.
- Einsele, W., 1936. Ueber die Beziehungen des Eisenkreislaufs zum Phosphatkreislauf um eutrophen See. *Archiv für Hydrobiologie Special Issues Advanced Limnology* 29, 664–686.
- Ferro, I., 2003. *Cycling of Iron and Manganese in Freshwater, Estuarine and Deep Sea Sediments*. University of Groningen.
- Francois, F., Gerino, M., Stora, G., Durbec, J.P., Poggiale, J.C., 2002. Functional approach to sediment reworking by gallery-forming macrobenthic organisms: modeling and application with the polychaete *Nereis diversicolor*. *Marine Ecology – Progress Series* 229, 127–136.
- Friedl, G., Wehrli, B., Manceau, A., 1997. Solid phases in the cycling of manganese in eutrophic lakes: new insights from EXAFS spectroscopy. *Geochimica et Cosmochimica Acta* 61, 275–290.
- Furrer, G., Wehrli, B., 1996. Microbial reactions, chemical speciation, and multicomponent diffusion in porewaters of a eutrophic lake. *Geochimica et Cosmochimica Acta* 60, 2333–2346.
- Gächter, R., Imboden, D., 1985. Lake restoration. In: Stumm, W. (Ed.), *Chemical Processes in Lakes*. John Wiley & Sons, pp. 365–388.
- Gächter, R., Meyer, J.S., 1990. Mechanisms controlling fluxes of nutrients across the sediment/water interface in a eutrophic lake. In: Bands, R., Giesy, J. (Eds.), *Fates and Effects of In-place Pollutants in Aquatic Ecosystems*. Lewis Publishing, Ann Arbor, pp. 131–162.
- Gächter, R., Meyer, J.S., 1993. The role of microorganisms in mobilisation and fixation of phosphorus in sediment. *Hydrobiologia* 253, 103–121.
- Gächter, R., Müller, B., 2003. Why the phosphorus retention of lakes does not necessarily depend on the oxygen supply to their sediment surface. *Limnology and Oceanography* 48, 929–933.
- Gächter, R., Stadelmann, P., 1993. *Sempachersee. Mitteilungen der Naturforschenden Gesellschaft Luzern*, p. 33.
- Gächter, R., Wehrli, B., 1998. Ten years of artificial mixing and internal phosphorus loading of two eutrophic lakes. *Environmental Science and Technology* 32, 3659–3665.
- Hecky, R.E., Campbell, P., Hendzel, L.L., 1993. The stoichiometry of carbon, nitrogen, and phosphorus in particular matter of lakes and oceans. *Limnology and Oceanography* 38, 709–724.
- Höhener, P., Gächter, R., 1993. Prediction of dissolved inorganic nitrogen (DIN) concentrations in deep, seasonally stratified lakes based on rates of DIN input and N removal processes. *Aquatic Sciences* 55, 112–131.
- Hunter, K.S., Wang, Y., Van Cappellen, P., 1998. Kinetic modeling of microbially-driven redox chemistry of subsurface environments: coupling transport, microbial metabolism and geochemistry. *Journal of Hydrology* 209, 53–80.
- Hupfer, M., Gächter, R., Giovanoli, R., 1995. Transformation of phosphorus species in settling seston and during early diagenesis. *Aquatic Science* 57, 305–324.
- Hupfer, M., Lewandowski, J., 2008. Oxygen controls the phosphorus release from lake sediments—a long-lasting paradigm in limnology. *International Review of Hydrobiology* 93, 415–432.
- Hupfer, M., Pothig, R., Brüggemann, R., Geller, W., 2000. Mechanical resuspension of autochthonous calcite (Seekreide) failed to control internal phosphorus cycle in a eutrophic lake. *Water Research* 34, 859–867.
- Katsev, S., Chaillou, G., Sundby, B., Mucci, A., 2007. Effects of progressive oxygen depletion on sediment diagenesis and fluxes: a model for the lower St. Lawrence River Estuary. *Limnology and Oceanography* 52, 2555–2568.
- Katsev, S., Rancourt, D.G., L'Heureux, I., 2004. dSED: a database tool for modeling sediment early diagenesis. *Computers and Geosciences* 30, 959–967.
- Katsev, S., Sundby, B., Mucci, A., 2006a. Modeling vertical excursions of the redox boundary in sediments: application to deep basins of the Arctic Ocean. *Limnology and Oceanography* 51, 1581–1593.
- Katsev, S., Tsandev, I., L'Heureux, I., Rancourt, D.G., 2006b. Factors controlling long-term phosphorus efflux from lake sediments: exploratory reactive-transport modeling. *Chemical Geology* 234, 127–147.
- Lasaga, A.C., Holland, H.D., 1976. Mathematical aspects of non-steady-state diagenesis. *Geochimica et Cosmochimica Acta* 40, 257–266.
- Li, J., Crowe, S.A., Miklesh, D., Kistner, M., Canfield, D.E., Katsev, S., 2012. Carbon mineralization and oxygen dynamics in sediments with deep oxygen penetration, Lake Superior. *Limnology and Oceanography* 56, 1634–1650.
- Matisoff, G., Wang, X.S., McCall, P.L., 1999. Biological redistribution of lake sediments by tubificid oligochaetes: *Branchiura sowerbyi* and *Limnodrilus hoffmeisteri/Tubifex tubifex*. *Journal of Great Lakes Research* 25, 205–219.
- Morse, J.W., Cornwell, J.C., 1987. Analysis and distribution of iron sulfide minerals in recent anoxic marine-sediments. *Marine Chemistry* 22, 55–69.
- Morse, J.W., Eldridge, P.M., 2007. A non-steady-state diagenetic model for changes in sediment biogeochemistry in response to seasonally hypoxic/anoxic conditions in the “dead zone” of the Louisiana shelf. *Marine Chemistry* 106, 239–255.
- Morse, J.W., Millero, F.J., Cornwell, J.C., Rickard, D., 1987. The chemistry of the hydrogen-sulfide and iron sulfide systems in natural waters. *Earth-Science Reviews* 24, 1–42.
- Mortimer, C.H., 1941. The exchange of dissolved substances between mud and water in lakes. *Journal of Ecology* 29, 280–329.
- Müller, B., Wang, Y., Dittrich, M., Wehrli, B., 2003. Influence of organic carbon decomposition on calcite dissolution in surficial sediments of a freshwater lake. *Water Research* 37, 4524–4532.
- Müller, B., Wang, Y., Wehrli, B., 2006. Cycling of calcite in hard water lakes of different trophic states. *Limnology and Oceanography* 51, 1678–1688.
- Müller, R., Stadelmann, P., 2004. Fish habitat requirements as the basis for rehabilitation of eutrophic lakes by oxygenation. *Fisheries Management and Ecology* 11, 251–260.
- Pallud, C., Van Cappellen, P., 2006. Kinetics of microbial sulfate reduction in estuarine sediments. *Geochimica et Cosmochimica Acta* 70, 1148–1162.
- Parfitt, R.L., 1989. Phosphate reactions with natural allophane, ferrihydrite, and goethite. *Journal of Soil Science* 40, 359–369.

- Poulton, S.W., Canfield, D.E., 2005. Development of a sequential extraction procedure for iron: implications for iron partitioning in continentally derived particulates. *Chemical Geology* 214, 209–221.
- Roden, E.E., Edmonds, J.W., 1997. Phosphate mobilization in iron-rich anaerobic sediments: microbial Fe(III) oxide reduction versus iron-sulfide formation. *Archiv für Hydrobiologie* 139, 347–378.
- Roden, E.E., Wetzel, R.G., 2002. Kinetics of microbial Fe(III) oxide reduction in freshwater wetland sediments. *Limnology and Oceanography* 47, 198–211.
- Schauser, I., Hupfer, M., Bruggemann, R., 2004. SPIEL—a model for phosphorus diagenesis and its application to lake restoration. *Ecological Modelling* 176, 389–407.
- Schauser, I., Hupfer, M., Bruggemann, R., 2006. Sensitivity analysis with a phosphorus diagenesis model (SPIEL). *Ecological Modelling* 190, 87–98.
- Schauser, I., Lewandowski, J., Hupfer, M., 2003. Decision support for the selection of an appropriate in-lake measure to influence the phosphorus retention in sediments. *Water Research* 37, 801–812.
- Sondergaard, M., Jensen, P.J., Jeppesen, E., 2001. Retention and internal loading of phosphorus in shallow, eutrophic lakes. *The Scientific World Journal* 1, 427–442.
- Stadelmann, P., 1988. Der Zustand des Sempachersees. *Wasser, Energie, Luft* 80, 81–96.
- Stumm, W., Morgan, J., 1996. *Aquatic Chemistry. An Introduction Emphasizing Chemical Equilibria in Natural Waters*. John Wiley & Sons, New York, 780 p.
- Sundby, B., Anderson, L.G., Hall, P.O.J., Iverfeldt, A., Vanderloeff, M.M.R., Westlund, S.F.G., 1986. The effect of oxygen on release and uptake of cobalt, manganese, iron and phosphate at the sediment–water interface. *Geochimica et Cosmochimica Acta* 50, 1281–1288.
- Tessier, A., Campbell, P.G.C., Blsson, M., 1979. Sequential extraction procedure for the speciation of particulate trace metals. *Analytical Chemistry* 51, 844–851.
- Urban, N.R., Dinkel, C., Wehrli, B., 1997. Solute transfer across the sediment surface of a eutrophic lake: I. Porewater profiles from dialysis samples. *Aquatic Sciences* 59, 1–25.
- Van Cappellen, P., Wang, Y., 1996. Cycling of iron and manganese in surface sediments: a general theory for the coupled transport and reaction of carbon, oxygen, nitrogen, sulfur, iron, and manganese. *American Journal of Science* 296, 197–243.
- Wehrli, B., Wüest, A., 1996. Zehn Jahre Seebelüftung—Erfahrungen und Optionen. *EAWAG News* 42D, 28–29.
- Wieland, E., Santschi, P.H., Hohener, P., Strum, M., 1993. Scavenging of Chernobyl Cs-137 and Natural Pb 210 in Lake Sempach, Switz. *Geochimica et Cosmochimica Acta* 57, 2959–2979.
- Wijsman, J.W.M., Herman, P.M.J., Middelburg, J.J., Soetaert, K., 2002. A model for early diagenesis processes in sediments of the continental shelf of the Black Sea. *Estuarine, Coastal and Shelf Science* 54, 403–421.